12-2009

Geotechnical Site Characterization Using Multi-channel Analysis of Rayleigh and Love Waves

James David Lane, Jr.
University of Tennessee - Knoxville

To the Graduate Council:

I am submitting herewith a thesis written by James David Lane, Jr. entitled "Geotechnical Site Characterization Using Multi-channel Analysis of Rayleigh and Love Waves." I have examined the final electronic copy of this thesis for form and content and recommend that it be accepted in partial fulfillment of the requirements for the degree of Master of Science, with a major in Civil Engineering.

Dayakar Penumadu, Major Professor

We have read this thesis and recommend its acceptance:

Richard Williams, Edwin Burdette

Accepted for the Council:
Carolyn R. Hodges

Vice Provost and Dean of the Graduate School

(Original signatures are on file with official student records.)

To the Graduate Council:

I am submitting herewith a thesis written by James David Lane, Jr. entitled "Geotechnical Site Characterization Using Multi-channel Analysis of Rayleigh and Love Waves." I have examined the final electronic copy of this thesis for form and content and recommend that it be accepted in partial fulfillment of the requirements for the degree of Master of Science, with a major in Civil Engineering.

Dayakar Penumadu, Major Professor

We have read this thesis and
recommend its acceptance:

Richard Williams

Edwin Burdette

Accepted for the Council:

Carolyn R. Hodges
Vice Provost and Dean of the Graduate School

(Original signatures are on file with official student records.)

Geotechnical Site Characterization Using Multi-Channel Analysis of Rayleigh and Love Waves

A Thesis
Presented for the
Master of Science
Degree
The University of Tennessee, Knoxville

James David Lane, Jr.
December 2009

DEDICATION

I would like to thank my parents James D. Lane and Sandy P. Lane for their firm support and encouragement in order to complete a graduate level degree.

ACKNOWLEDGEMENTS

I would like to thank the University of Tennessee's College of Civil and Environmental Engineering and the College of Mechanical, Aerospace, and Biomedical Engineering for their financial support. I would also like to thank the professors in charge of this project, Dr. Dayakar Penumadu and Dr. Richard Williams. Without their support and guidance, none of this research work and thesis would have come to fruition. My fellow graduate research assistant, William Ragland, was instrumental in the project by providing his vast technical knowledge, programming skills, and help with the seismic surveys. I would also like to thank Ken Thomas for his logistical support and Larry Roberts for his assistance in operating the drill rig and for the setup of the seismic surveys.

ABSTRACT

The Multi-Channel Analysis of Surface Waves (MASW) is a technique in which surface waves can be analyzed to determine soil shear wave velocity profiles with depth. The shear wave velocity of soil can be used to calculate the shear modulus, which is an important geotechnical engineering parameter. Site surveys were conducted and analyzed located at a location on the flood plain of the Tennessee River. The flood plain consists of a thin layer of soil above rigid (Knox Dolomite) bedrock and exhibited strong stratification. Three different aspects of MASW data acquisition and analysis are presented in the study. The first aspect is the response correction of the classical horizontal and vertical component geophone and its effects on surface wave dispersion; the second aspect is the effect of Rayleigh wave MASW data acquisition, analysis, and modeling as influenced by Rayleigh wave guides; the third aspect is the use of MASW and Love wave data acquisition, analysis, and modeling. MASW is performed using a seismic source and geophones (velocity sensor) without correcting the amplitude and phase errors induced by the equivalent single degree of freedom response function representing the mechanical response of a given velocity sensor. Geophones were experimentally tested in the laboratory to determine their natural frequency, damping ratio, and transduction constants. The results from these tests were mathematically corrected for their mechanical response and compared to uncorrected and corrected field data. Several seismic sources and various source-offset distances were evaluated to determine their effects on Rayleigh wave dispersion. Rayleigh waves, guided in a layer, were interpreted to have a profound influence on the Rayleigh wave dispersion data obtained using different seismic sources and source-offset distances. Results

from Love wave data analysis produced superior dispersion data in comparison to the dispersion data obtained from Rayleigh wave data, making interpretation much more certain.

TABLE OF CONTENTS

Chapter 1: Research Background and Objectives....1
Research Background and Introduction....1
Research Objectives....3
Report Organization....4
Chapter 2: Use of Multi-Channel Analysis of Surface Waves (MASW) for Geotechnical Site Characterization Using Corrected Triaxial Geophones....5
Abstract....6
Introduction....7
Geophone Theory....9
Geophone Response Calibration....11
Geophone Output Correction....11
Field Test....12
Effect of Source Type on Rayleigh Wave Dispersion....14
Results and Discussion....16
Conclusions....17
References....19
Appendix....22
Tables....23
Figures....24
Chapter 3: Multi-Channel Analysis of Surface Waves (MASW) for Thin Soil above Bedrock for a Flood Plain Site of Tennessee River....38
Abstract....39
Introduction....40
Survey Setup....42
Comparison of Different Seismic Sources....43
Source Offset Distance....44
Geophone Orientation....45

MASW Survey 45
Rayleigh-Lamb Model 47
MASW Profile: Results from SurfSeis 48
Number of Layers in the Model 49
Conclusions 49
References 51
Appendix 54
Tables 55
Figures 56
Chapter 4: Love Wave Dispersion, Analysis, and Modeling via the Multi-Channel Analysis of Surface Waves (MASW) Technique 68
Abstract 69
Introduction 70
Site Location 71
Survey Setup 73
Love Wave MASW Survey 73
Constraints on Depth to Bedrock 75
Conclusions 76
References 77
Appendix 80
Tables 81
Figures 82
Conclusions and Recommendations for Future Research 90
Conclusions 90
Recommendations for Future Research 92
Vita 93

LIST OF TABLES

Table 2.1. Geophone parameter summary and wellness of curve fit. 23
Table 3.1. Shear velocities (m/s) as a function of source point and depth for a 10 layer inversion. The basal layer is a half-space. 55
Table 4.1. Shear velocities (m/s) as a function of source point and depth for a 33 layer inversion. Knox dolomite bedrock is at the base of the soft sediment layers. The depth column shows depth to the bottom of the layer. 81

LIST OF FIGURES

Figure 2.1. Typical MASW configuration (KGS 1998).....24
Figure 2.2. Background seismic waves and respective time series data (KGS 1998).....24
Figure 2.3. Geophone Schematic (Brincker 2005). 25
Figure 2.4. Geophone modeled as a single degree of freedom system. 25
Figure 2.5. Geophone Sensitivity vs. the ratio of excitation frequency to geophone natural frequency for various damping ratios.....26
Figure 2.6. Geophone Sensitivity vs. the ratio of excitation frequency to geophone natural frequency for various damping ratios.....26
Figure 2.7. Mark Products RS-1000 10Hz vertical geophone (blue) and L-28LBH 4.5Hz horizontal geophone (orange) mounted on the MTS 858 servo-hydraulic device.....27
Figure 2.8. Seismic data before and after correction for the geophone response. 28
Figure 2.9. Uncorrected vertical component Rayleigh wave dispersion image. 29
Figure 2.10. Corrected vertical component Rayleigh wave dispersion image. 29
Figure 2.11. MASW site location. 30
Figure 2.12. Left – Source coupling, Right – Receiver coupling. 30
Figure 2.13. Measurement scheme of vertical and horizontal geophones for Rayleigh waves. 31
Figure 2.14. Measurement scheme of vertical and horizontal geophones for Love waves. 31
Figure 2.15. Top: Hammer and Plate source, Bottom left: 22.5kg Sand bag source, Bottom Center: Hammer and 45° wooden block, Bottom Right: ELECTRO-SEIS® Vibrator.....32
Figure 2.16. Vertical uncorrected Rayleigh wave dispersion image from 22.5kg bag of sand source.....33
Figure 2.17. Vertical corrected Rayleigh wave dispersion image from 22.5kg bag of sand source.....33
Figure 2.18. Vertical geophone uncorrected Rayleigh wave dispersion image from Hammer and Plate source. 34
Figure 2.19. Vertical geophone response corrected Rayleigh wave dispersion image from Hammer and Plate source. 34
Figure 2.20. Vertical uncorrected Rayleigh wave dispersion image from Hammer and 45° wooden block source. 35
Figure 2.21. Vertical corrected Rayleigh wave dispersion image from Hammer and 45° wooden block source. 35
Figure 2.22. Vertical uncorrected Rayleigh wave dispersion image from ELECTRO-SEIS® vibrator source.....36
Figure 2.23. Vertical corrected Rayleigh wave dispersion image from ELECTRO-SEIS® vibrator source.....36
Figure 2.24. Transverse horizontal geophone uncorrected Love wave dispersion image from Hammer and 45° wooden block source. 37
Figure 2.25. Transverse horizontal geophone corrected Love wave dispersion from Hammer and 45° wooden block source.....37

Figure 3.1. Site location. Survey site was on the flood plain of the Tennessee River, on the University of Tennessee Agriculture Campus. 56
Figures 3.2. Example Rayleigh wave dispersion curves (no wave guide), fundamental mode and higher modes. 56
Figures 3.3. Example Rayleigh-Lamb wave dispersion curves (with wave guide), fundamental mode and higher modes. Subsurface velocities as in Fig. 3.2, but the effect of practically rigid bedrock is included. Notice cutoff in fundamental mode at ~10 Hz 57
Figure 3.4. Sources and receivers. Shallow holes were used to improve coupling. 57
Figure 3.5. Measurement scheme of vertical and horizontal geophones for Rayleigh waves 58
Figure 3.6. Seismic sources. Top: sledge hammer and aluminum plate. Bottom left: 22.5 kg bag of sand. Bottom center: sledge hammer and 45° wooden block. Bottom right: ELECTRO-SEIS® vibrator....58
Figure 3.7. Dispersion image obtained using SurfSeis. Source offset of 5 m using sledge hammer and aluminum plate seismic source placed flat on the soil. 59
Figure 3.8. Dispersion image obtained using SurfSeis. Source offset of 5 m using 22.5 kg bag of sand seismic source dropped from a height of 1 m. 59
Figure 3.9. Dispersion image obtained using SurfSeis. Source offset of 5 m using sledge hammer and 45° wooden block seismic source. 60
Figure 3.10. Dispersion image obtained using SurfSeis. Source offset of 5 m using ELECTRO-SEIS® vibrator seismic source. 60
Figure 3.11. Dispersion image obtained using SurfSeis. Source offset of 1 m using hammer and 45° wooden block seismic source. 61
Figure 3.12. Dispersion image obtained using SurfSeis. Source offset of 16.5 m using 22.5 kg bag of sand seismic source. 61
Figure 3.13. Dispersion image obtained using SurfSeis. Source offset of 28 m using 22.5 kg bag of sand seismic source. 62
Figure 3.14. Horizontal, radially oriented geophone dispersion image obtained using SurfSeis. Source offset of 5 m using 22.5 kg bag of sand seismic source....62
Figure 3.15. Horizontal, radially oriented geophone dispersion image obtained using SurfSeis. Source offset of 5 m using sledge hammer and 45° wooden block seismic source. 63
Figure 3.16. Seismic data example. One of 13 such records in the MASW data set. Left- vertical geophones. Right - Horizontal (radial) geophones. Shown are the first 250 ms from 1 sec records. 64
Figure 3.17. Fundamental mode dispersion curve (white squares) interepreted from the dispersion image for record #1. Solid lines- Rayleigh wave dispersion. Dashed lines- Rayleigh-Lamb dispersion. (see text)....65
Figure 3.18. Result of MASW analysis: a 2-D shear velocity profile 65
Figure 3.19. Shear velocity profile (Fig. 3.18) with overlay of individual 1-D inversion results. 66
Figure 3.20. Shear velocity profile results based on number of layers at source point 1....67
Figure 3.21. Shear velocity profile results based on number of layers at source point 13....67

Figure 4.1. Surface wave data were recorded on the flood plain of the Tennessee River at Knoxville, TN. 82
Figure 4.2. Example Rayleigh-Lamb (waveguide) wave dispersion curves, fundamental mode and higher modes. Results in Table 3.1 (i.e. number of soil layers, shear velocities, depth to bedrock) used for starting model except Knox Dolomite properties were used for the bottom layer. 82
Figure 4.3. Example Love wave dispersion curves, fundamental mode and five higher modes. Starting model used 10 m depth to bedrock, 125 m/s near surface shear velocity monotonically increasing to 450 m/s for deep shear velocity. 83
Figure 4.4. Measurement scheme for vertical and horizontal geophones for Love wave detection 84
Figure 4.5. Left: Hammer and 45° wooden block source, Right: Geophone coupling location 84
Figure 4.6. Seismic data example. Left - vertical geophones. Right - Horizontal (transverse) geophones. Shown are the first 250 ms from 1 sec records. 85
Figure 4.7. Baseline dispersion image obtained by analyzing the data from 24 horizontal geophones as a single seismic data record. White squares show the phase velocities interpreted at selected frequencies for the fundamental mode. Compare to the corresponding dispersion image for Rayleigh wave data (Fig. 3.9). 86
Figure 4.8. Baseline dispersion image (Fig. 4.8) with fundamental and higher mode Love wave dispersion curves (heavy black lines) that result from inversion of the dispersion data (white squares in Fig. 4.8). Note that the first higher mode, weakly visible in the dispersion image, is also satisfied by inversion of only the fundamental mode data. Thin black lines right and left of the heavy black dispersion curves are for bedrock depths at 12 and 13 m, respectively. Heavy curves are for 12.5 m bedrock depth. 87
Figure 4.9. Result of MASW analysis. The profile has a horizontal exaggeration of approximately 4X. The distance from the left edge to the right edge is 12 m, almost the same as the vertical span of 12.5 m. 88
Figure 4.10. Stack of 13 individual dispersion images to enhance the higher modes. The first higher mode, visible in Figure 4.9 is no can no longer be seen, but dispersion of the second and third higher modes is revealed. Note that inversion of only the fundamental mode data also satisfies the visible higher modes. 89

Chapter 1: Research Background and Objectives

Research Background and Introduction

Evaluation of near-surface engineering properties of soil for geotechnical site characterization is typically performed using invasive techniques such as mechanical borehole coring. These techniques are tried and true, providing discrete soil samples for evaluation in laboratory environments. However, invasive techniques are not practical or applicable in all geotechnical site characterization surveys, such as large areas of investigation or environmentally contaminated sites. Non-invasive, near-surface geotechnical site characterization can be performed without disturbing the soil. One particular non-invasive method of geotechnical site characterization is to utilize seismic surveys via multi-channel analysis of surface waves (MASW).

The traditional MASW technique evaluates a particular kind of surface shear wave, the Rayleigh wave. The MASW method utilizes Rayleigh wave phase velocity dispersion, where the data are converted from the offset – time domain to the frequency – phase velocity domain. Rayleigh waves are a logical choice because they can be easily imparted into the soil via a vertical seismic source. Data acquisition consists of a vertical seismic source, multiple geophones situated along a straight line at equal spacing, and a seismograph to record time – series data, known as a shot record. The shot record data are imported into commercial MASW processing software, SurfSeis (KGS 2006), in order to determine phase velocity dispersion curves. From SurfSeis, the fundamental mode Rayleigh wave dispersion curve is determined

and then inverted to produce shear wave velocity profiles with depth. Shear moduli for the soil can then be obtained from the interpreted shear wave velocities.

The shear modulus is an important geotechnical engineering property in that it describes soil response to shearing strains. Dynamic loading from wind, equipment vibrations, or earthquakes lead to a buildup of shear strains that would strongly influence the designs of civil engineering structures such as foundations. The fundamental equation for shear modulus is the ratio of shear stress to shear strain and can be obtained by multiplying the square of the shear wave velocity with the density of the soil.

Geotechnical site characterization using multi-channel analysis of Rayleigh and Love waves is more robust in that both surface waves are evaluated to determine the shear velocities of the sub-surface. Rayleigh waves propagate as ground-roll in an elliptical motion in planes normal to the surface in the direction of propagation and are dependent upon Poisson's ratio. Love waves propagate in the horizontal direction as transverse waves, perpendicular to the direction of propagation, are independent of Poisson's ratio, are guided in an elastic layer, and are non-existent in a half space. Rayleigh wave dispersion and inversion analysis reveal vertical shear velocities (Vsv) of the sub-surface, whereas Love wave dispersion and inversion analysis disclose horizontal shear velocities (Vsh) of the sub-surface. In an isotropic homogeneous soil, one would expect both shear velocities to be equal. However, in the case of true earth environments, soil stratification is far from isotropic and homogeneous; thus, obtaining shear velocities in both the vertical and horizontal direction can yield additional information to enhance the confidence in making geotechnical design decisions.

Research Objectives

A large amount of the previous MASW work has concentrated on the use of fundamental mode Rayleigh wave dispersion obtained using vertical geophones. The first research objective was to evaluate classical geophone response correction and make comparisons between uncorrected and corrected 3-component Rayleigh and Love wave data. The second research objective was to evaluate Rayleigh wave dispersion in the case of thin soil above rigid (Knox Dolomite) bedrock at a specific site located within the flood plain of the Tennessee River. The third research objective was to evaluate Love wave dispersion and modeling parameters.

The geophone response correction and comparisons between uncorrected and corrected 3-component Rayleigh and Love wave data were conducted in both the laboratory and survey site. Vertical and horizontal component geophone properties were obtained by using a servo-hydraulic material testing system along with a reference accelerometer and seismograph. Given that geophones measure velocity of ground motion, a transfer function was used so that the geophone output was proportional to acceleration. The magnitude of the transfer function was then used to determine geophone properties. A field survey was conducted in order to obtain 3-component (triaxial) Rayleigh and Love wave data. Field survey data was input into a computer software program that allowed for the correction of time series data. The uncorrected and corrected data were input into MASW data processing software to compare soil dispersion from the triaxial data. Comparisons were made between the uncorrected and corrected data in addition to conclusions regarding geophone response correction at the survey site.

Evaluation of Rayleigh wave dispersion in the case of thin soil above rigid (Knox Dolomite) bedrock located within the flood plain of the Tennessee River was also examined.

The MASW survey site is expected to exhibit the characteristics of a soft soil layer over high velocity bedrock. Optimum site specific parameters such as seismic source, source to first receiver offset, and geophone orientation were determined for successful fundamental mode Rayleigh-Lamb wave dispersion curve extraction. A great level of uncertainty was involved in interpreting the fundamental mode Rayleigh-Lamb wave dispersion curves because of a limited frequency range (<15 Hz) of phase velocity dispersion. The interpreted fundamental mode Rayleigh wave curves were inverted to obtain shear velocity profiles with depth.

Evaluation of Love wave phase velocity dispersion was based on the results of horizontal component geophone phase velocity dispersion. The Love wave phase velocity dispersion consistently produced a continuous fundamental mode curve over a greater frequency range, including lower frequencies (<10 Hz) much more clearly than the Rayleigh wave phase velocity dispersion. The Love wave data was analyzed using Computer Programs in Seismology, unpublished software from the University of St. Louis (Hermann 1996), in which several starting models were employed to fit fundamental mode curves to phase velocity dispersion to determine depth to bedrock. The fundamental mode Love wave curves were then inverted to produce a two dimensional shear velocity profile. Comparisons were made between the two dimensional Rayleigh and Love wave shear velocity profiles.

Report Organization

The report is organized into five chapters with an introduction and three articles for potential journal publication, conclusions are presented at the end of each article as well as final summary conclusions at the end of the report.

Chapter 2: Use of Multi-Channel Analysis of Surface Waves (MASW) for Geotechnical Site Characterization Using Corrected Triaxial Geophones.

This chapter is slightly revised version of a paper by J. David Lane, William Ragland, Richard Williams, and Dayakar Penumadu entitled, "Use of Multi-Channel Analysis of Surface Waves (MASW) for Geotechnical Site Characterization Using Corrected Triaxial Geophones" presented at the Symposium on the Application of Geophysics to Engineering and Environmental Problems (SAGEEP) conference at Philadelphia, PA in April, 2008.

My primary contributions to this paper include: (1) evaluation of the topic and development of the problem to study the benefits of geophone response correction, (2) detailing the benefits of obtaining multi-axial surface wave data to include the use of both Rayleigh and Love Waves, (3) obtaining and interpretation of published literature, (4) performing all of the laboratory and field experiments, (5) comparing and analyzing laboratory results between the excitation device and various testing equipment, and (6) performing the writing necessary for manuscript preparation.

Abstract

Surface wave methods are often used to map shear wave velocity variation of soil as a function of depth. Typically, either a spectral analysis of surface waves (SASW), using two geophones, or multi-channel analysis of surface waves (MASW), using 12 or more geophones, is performed using vertical component geophones. Both analyses are performed using data slightly distorted by the mechanical response of the geophone. In this chapter MASW was utilized for evaluating the shear wave velocity with depth for a geotechnical site in Knoxville, TN. Field records of various geophones measured using a 48 channel seismograph associated with a MASW survey are corrected using experimentally determined transfer functions. MASW

data were collected using a 1-meter geophone spacing along with several types of seismic excitation sources at a 5-meter source-offset distance. The data were collected using 10 Hz vertical and 4.5 Hz horizontal geophones, which are calibrated against a reference piezoelectric accelerometer using a servo-hydraulic testing system. A comparison of uncorrected and corrected 3-component surface wave data collected at a soft soil site on the Tennessee River flood plain is presented in this chapter.

Introduction

The multi-channel analysis of surface waves (MASW) method (Park et al., 1999) has emerged as a valuable technique for non-invasive seismic testing to evaluate shear-wave velocity or stiffness of the ground and subsurface (Figure 2.1, all tables and figures are located in the Chapter 2 Appendix) for geotechnical site characterization (Penumadu and Park, 2005; Long and Donahue, 2007). This method analyzes dispersion properties of seismic surface waves (fundamental-mode Rayleigh waves) propagating horizontally along the ground surface directly from impact source to vertical receivers. Shear wave velocity information is typically presented in 1-D (depth) or 2-D (depth and surface location) format. The fundamental framework of the MASW method is based on the multi-channel recording and analysis approach long used in seismic exploration surveys (Telford et al., 1976) that can discriminate useful signals against all other types of noise (Figure 2.2). The noise may make up a significant portion of the recorded data, which calls into question the validity of survey results if they are not taken into account.

Several cases of its applications for different purposes such as geophysical, geological, environmental, and geotechnical engineering projects have been studied. Miller et al. (1999)

successfully applied the MASW technique to map weak spots in bedrock. Ivanov et al. (2006) used MASW to delineate a shallow fault zone and dipping bedrock strata using MASW. A 3-D shear wave velocity mapping was also accomplished using the MASW method at a military weapon test site in Arizona (Miller et al., 2003). Ivanov et al. (2003) and Park et al. (1998b) used the method to detect underground anomalies. MASW was also used to evaluate the effectiveness of a compaction operation conducted as a soil remediation tool at a construction site (Park et al., 2003).

Traditionally, MASW relies only on Rayleigh waves recorded using vertical component geophones. However, site specific characteristics such as shallow layers of soft soil situated over high velocity bedrock may produce other types of surface waves, such as Love waves, in addition to Rayleigh waves. For this reason, it is believed the use of three-component data for analysis results in an improved understanding of the subsurface. In either case, all collected data should be corrected to account for the mechanical response of the geophones.

Geophones are highly sensitive motion transducers that measure velocity response to seismic excitation. The problem with measuring velocity using geophones is that the linear frequency range is limited to frequencies above the natural frequency of the geophone. Brincker et al. (2005) corrected for the mechanical response of vertical geophones by digital correction. Implementation of transfer functions digitally allowed for the linearization of the geophone signal two decades of frequency range below the geophones natural frequency. This allows the user to obtain data below the natural frequency of the geophone as well as measure displacement, velocity, or acceleration within a larger dynamic range (Brincker et al. 2005). However, their study did not consider the effect of various types of seismic excitation sources.

Geophone Theory

A geophone is a device that measures ground motion in the direction of its cylindrical axis. Inside an exterior housing, a coil is suspended by leaf springs around a permanent magnet, as illustrated in Figure 2.3. As the geophone housing is excited by ground excitation, the coil moves relative to the magnet producing a voltage. Faraday's Law states that the voltage across the coil is proportional to the change in flux through the coil with respect to time. For small displacements, U, the change in flux, Φ, is constant, and thus the voltage, V, across the coil is directly proportional to the velocity of the coil as shown in equation (1) in the Laplace domain, where G is a transduction constant referred to as the sensitivity of the geophone.

$$V = -\frac{\partial \varphi}{\partial t} = -\frac{\partial \varphi}{\partial t}\frac{\partial u}{\partial t} = -G\dot{U} = -GsU \tag{1}$$

φ is flux, t is time, and G is the transduction constant. A geophone can be modeled mathematically as a single degree of freedom system as shown in equation (2) and illustrated in Figure 2.4, where m is mass, u is the displacement of the mass, c is the damping coefficient, k is the stiffness of the spring, and x is the ground displacement. Using the Laplace transform, the motion of the mass is described by the transfer function given in equation (3).

$$m\ddot{u} + c\dot{u} + ku = -m\ddot{x} \tag{2}$$

$$H(s) = \frac{U(s)}{F(s)} = \frac{U}{\ddot{X}} = \frac{-1}{s^2 + 2\zeta\omega_n s + \omega_{n^2}} \tag{3}$$

where $\frac{c}{m} = 2\zeta\omega_n$, $\frac{k}{m} = \omega_{n^2}$, and $s = i\omega$.

Incorporating Faraday's Law and integrating the acceleration term in the denominator once, after simplification, the transfer function of a geophone for velocity is determined as shown in equation (4) where G is the transduction constant of the geophone, ω_n is the natural frequency of the geophone, ζ is its damping ratio, and ω is the excitation frequency.

$$H(i\omega) = \frac{V(\omega)}{\dot{X}(\omega)} = \frac{G\left(\frac{\omega}{\omega_n}\right)^2}{\left[1 - \left(\frac{\omega}{\omega_n}\right)^2\right] + 2i\zeta\frac{\omega}{\omega_n}} \tag{4}$$

The geophone transfer function is commonly presented in this form because the output voltage is approximately constant at frequencies above the natural frequency of the geophone. At frequencies below the geophone's natural frequency, the output voltage is not constant with respect to velocity for various damping ratios as shown in Figure 2.5. If the decrease in sensitivity below the geophone's natural frequency is not accounted for, measured vibrations with frequencies in this range will be misrepresented in terms of amplitude. Geophones also introduce phase shifts into measured data at frequencies near the geophone's natural frequency as shown in Figure 2.6. If these phase shifts are not accounted for, the measured vibration will not be in phase with the actual input vibration. It is particularly important to correct for phase shifts when geophones with different response characteristics (for example, 4.5 Hz and 10 Hz) are used as was done in this study. Considering these factors, magnitude and phase errors present in geophone output can be easily corrected by dividing each frequency component of the output signal by the geophone's transfer function evaluated at the corresponding frequency.

Geophone Response Calibration

Three parameters are needed for the geophone transfer function: (1) the transduction constant G, (2) the natural frequency ω_n, and the damping ζ. These parameters were determined experimentally in the laboratory using a Brüel & Kjær 4371 V reference accelerometer. A Mark Products LRS-1000 10Hz vertical geophone, a Mark Products L-28LBH 4.5Hz horizontal geophone, and the reference accelerometer were mounted together on a single steel plate which was then attached to Material Testing Systems (MTS) 858 servo-hydraulic equipment as depicted in Figure 2.7. The MTS is only capable of producing vertical motion, so the horizontal geophone was mounted at an inclination of 6° for comparison to the vertical geophone and reference accelerometer.

On the MTS, the geophones and reference accelerometer were subjected to known, constant sinusoidal motions at frequencies from 2 to 30 Hz, at constant amplitude, and the signal voltages were recorded using a Geometrics, Inc. model RX-48 seismograph. Taking the Fourier transforms of the geophone signals, and recasting equation (4) in terms of acceleration instead of velocity, the geophone parameters were determined using the Levenberg-Marquardt algorithm in MATLAB® (Mathworks 2007). The geophone calibration parameters thus determined are presented in Table 2.1.

Geophone Output Correction

After determination of the geophone parameters, the seismic field records can be easily corrected for the mechanical response of the geophones to obtain a true records of velocity via equation (4). The fast Fourier transform (FFT) was used to transform the time domain signal

collected in the field to the frequency domain, the correction was applied in the frequency domain, then the inverse fast Fourier transform (IFFT) was used to transform back to the time domain. An example of the effect of correcting the seismic data for the geophone response is shown in Figure 2.8

Figures 2.9 and 2.10 show phase velocity dispersion images, using the same seismic field records, before and after correction for the geophone response. Observing the figures, there is a distinct difference in amplitude between the uncorrected and corrected dispersion curves. This is a direct result of the correction procedure which amplifies frequency components in the field data. Comparing Figures 2.9 and 2.10, the corrected dispersion curve not only shows a better defined fundamental mode, but also shows a better defined higher mode curve.

Field Test

The test site chosen for this study was located in the flood plain of the Tennessee River at the University of Tennessee – Knoxville agricultural farm as shown in Figure 2.11. The flood plain is expected to exhibit a thin, soft low velocity soil layer over a high velocity bedrock layer. The bedrock is Knox dolomite (Cattermole, 1958). The S-wave velocity of the Knox dolomite is not known at this particular location, but is thought to be in the 3000-4000 m/s range. This is well suited for research as it proves to be a typical geophysical survey site in which various background noise sources associated with an urban city environment interferes with survey data collection. All collected data was processed using SurfSeis (KGS 2006), after geophone response correction, utilizing guidelines recommended by the Kansas Geological Survey (KGS 1998).

In order to enhance the seismic signal from four different impact sources and ensure no organic material remained, overburden from locations of geophones and source at the site was removed as shown in Figure 2.12. Removal of the overburden and topsoil eliminates the damping and resonant effects of the plant root structure as well as the voids between the geophone plate and the ground surface. Figure 2.12 shows, as an example, the source and receiver coupling locations. The first geophone was located 5 meters from the excitation source, known as the offset distance, and geophones were spaced at 1-meter intervals for twelve meters.

Rayleigh waves are easily generated by a vertical impact source and move in a circular or elliptical path in the direction of propagation. Theoretically, vertically oriented geophones and radially oriented horizontal geophones will measure Rayleigh wave data. However, field trials by experiment concluded that Rayleigh wave data are better obtained through the use of vertically oriented geophones. The field survey setup and visual representation for Rayleigh wave detection is shown in Figure 2.13.

Love waves are horizontally dispersing surface waves that are typically not measured by a vertical impact source. Horizontal transverse geophone data should result in different dispersion curves because Love wave phase velocities are different from Rayleigh wave phase velocities. Therefore, in order to measure Love wave dispersion, the geophone plates are rotated 90 degrees and the hammer and 45° wooden block source are used. The field survey setup and visual representation for Love wave detection is shown in Figure 2.14.

Effect of Source Type on Rayleigh Wave Dispersion

Four different seismic excitation sources (Figure 2.15) were used during the survey and are listed in order of ease of mobilization and utilization: a 22.5 kilogram sand bag, hammer and plate, hammer and 45° wooden block, and an ELECTRO-SEIS® vibrator. An uncorrected and corrected dispersion curve for each excitation source is illustrated in Figures 2.16 through 2.25. A description between each uncorrected and corrected dispersion data is presented.

Uncorrected and corrected Rayleigh wave dispersion data obtained from vertically oriented geophones using the 22.5 kilogram sand bag seismic source are shown in Figures 2.16 and 2.17. The uncorrected Rayleigh wave dispersion does not produce a well defined fundamental mode curve. There is an abrupt cutoff at 18 Hz between phase velocities of 300-500 m/s for what appears to be the fundamental mode curve. A higher mode curve is present starting at around 28 Hz continuing to 60 Hz, ranging in phase velocities from 400 m/s to 250m/s. The corrected dispersion curve shows a higher relative amplitude fundamental mode as well as a higher mode. The fundamental mode is shown starting at 8 Hz and continuing to approximately 24 Hz with a phase velocity range of 450 m/s to 180 m/s. There is an abrupt cutoff in the dispersion data at 24 Hz in between the fundamental mode and an additional higher mode. The 22.5 kilogram sand bag produces high relative amplitude data throughout a wide range of frequencies as shown in Figure 2.17.

Uncorrected and corrected Rayleigh wave dispersion data obtained from vertically oriented geophones using the hammer and plate seismic source are displayed in Figures 2.18 and 2.19. The uncorrected Rayleigh wave dispersion does not produce a continuous fundamental mode curve with spots of high relative amplitude between 11 Hz and 23 Hz at phase velocities

between 500 to 250 m/s. Higher mode dispersion is also visible between 30 Hz and 60 Hz from phase velocities of 400 m/s to 250 m/s. The corrected dispersion curve for the hammer and plate is shown in Figure 2.19. Both the fundamental and next higher mode is visible in the figure. The fundamental mode curve occurs between 8 Hz and 24 Hz, with small discontinuity near 17 Hz. The cutoff between the fundamental mode and higher mode is near 24 Hz. Notice that there is also some relative amplitude discontinuity in the higher mode dispersion curve.

Uncorrected and corrected Rayleigh wave dispersion data obtained from vertically oriented geophones using the hammer and 45° wooden block seismic source are illustrated in Figures 2.20 and 2.21. The uncorrected Rayleigh wave fundamental mode dispersion is discontinuous between 13 Hz and 23 Hz at phase velocities of 500 m/s and 250 m/s. A discontinuous higher mode is visible between 27 Hz and 60 Hz at phase velocities of 400 m/s and 150 m/s. The corrected fundamental dispersion curve is consistent with respect to relative amplitude between 11 Hz and 24 Hz at phase velocities between 500 m/s and 250 m/s. The higher mode shows areas of discontinuity with a cutoff between the fundamental and higher modes near 24 Hz. Since only a component of vertical energy is imparted to the soil, one would expect the dispersion curve to be different relative to the other direct vertical sources. However this is not the case.

Uncorrected and corrected Rayleigh wave dispersion data obtained from vertically oriented geophones using the ELECTRO-SEIS® vibrator seismic source are illustrated in Figures 2.22 and 2.23. The uncorrected Rayleigh wave fundamental mode dispersion is discontinuous from approximately 12 Hz to 28 Hz at phase velocities between 500 m/s to 250 m/s. A higher mode is visible between 40 Hz and 56 Hz at a constant phase velocity of 250 m/s. The corrected

dispersion curve enhances some of the relative amplitudes between 11 Hz to 28 Hz at phase velocities of 600 m/s to 250 m/s. The same higher mode is visible between 45 Hz and 57 Hz at a constant phase velocity of 250 m/s.

Uncorrected and corrected Love wave dispersion data obtained from transverse horizontal oriented geophones utilizing the hammer and 45° wooden block seismic source are shown in Figures 2.24 and 2.25. The uncorrected Love wave fundamental mode dispersion is continuous from 7 Hz to 50 Hz at phase velocities of 600 m/s to 175 m/s, with what appears to be an artifact at around 5 Hz. The corrected Love wave fundamental mode dispersion is continuous from about 8 Hz to 50 Hz at phase velocities of 350 m/s to 125 m/s. Neither the uncorrected or corrected Love wave dispersion provided any additional higher mode dispersion information.

Results and Discussion

Based on the Rayleigh wave dispersion results obtained using various excitation sources all of the dispersion data are relatively the same and are somewhat ambiguous as far as selecting definitive points corresponding to the highest energy content leading to a dispersion curve. In theory, geophone response correction should enhance the dispersion data at frequencies below the natural frequencies of the geophones. However, this is not the case at this particular site due to the lack of longer wavelength propagation in the thin soil layer overlaying the high velocity bedrock. The geophone response correction does enhance the continuity of dispersion data above the natural frequency of the geophones.

A comparison between Rayleigh and Love wave dispersion yields a significant difference in the quality of data. Selecting points to delineate the fundamental mode Rayleigh wave data for all the sources would be difficult to perform with confidence. There is quite a bit of uncertainty at lower frequencies and it would be easy to make incorrect fundamental mode dispersion picks which would results in an incorrect shear velocity soil profile after subsequent inversion. The Love wave dispersion is much cleaner and picking fundamental mode Love wave dispersion curve picks could be performed with much more confidence at this particular location.

The acquisition of both Rayleigh and Love wave data is recommended to enhance the practitioner's confidence in determining subsurface geotechnical properties. If only Rayleigh wave data were obtained from this site, it would be very difficult to model an accurate subsurface profile based on less than ideal fundamental mode dispersion data. The collection of Love wave data elicited a very clean and easy to decipher fundamental mode dispersion curve regardless of data corrected for geophone response. Computer software is publicly available for the evaluation of both Rayleigh and Love wave fundamental and higher mode dispersion, inversion, and subsurface modeling whereas SurfSeis is only able to calculate fundamental mode Rayleigh wave dispersion.

Conclusions

1. In theory, correction for geophone response should enhance dispersion data at frequencies lower than the geophone's natural frequency resulting in a better defined fundamental mode Rayleigh wave dispersion curve at these lower frequencies. However, this was not observed due to the nature of the geotechnical

site used in the study, because Rayleigh waves with longer wavelengths (or low frequency) do not propagate within the thin soil layer over high velocity bedrock.

2. Although correcting data for geophone response did not have much effect at this particular field study site, the benefits outweigh the time involved and may elicit important data below the natural frequency of the geophones at sites where longer wavelengths are able to propagate.
3. Love wave data yields better fundamental mode dispersion than Rayleigh waves at this particular site.
4. The benefits of obtaining both Rayleigh and Love wave data enhance the determination of subsurface geotechnical properties.

References

Brincker, R., Lagö, T.L., Andersen, P., and Ventura, C., 2005, Improving the Classical Geophone Sensor Element by Digital Correction, ftp://ftp.svibs.com/Download/Literature/Papers/2005/2005_1.pdf

Cattermole, J.M. 1958, Geology of the Knoxville Quadrangle, Tennessee, Geologic Quadrangle Map GQ-115, US Geological Survey

Ivanov, J., Miller, R.D., Lacombe, P., Johnson, C.D., and Lane Jr., J.W., 2006, Delineating a shallow fault zone and dipping bedrock strata using multi-channel analysis of surface waves with a land streamer, Geophysics 71(5), A39-A42

Ivanov, J., R.D. Miller, C.B. Park, and N. Ryden, 2003, Seismic search for underground anomalies, [Exp. Abs.]: Soc. Expl. Geophys., NSG3.2

Kansas Geological Survey (KGS), 2006, SurfSeis [computer software], Ver. 2.05

Kansas Geological Survey (KGS), 1998, Introduction to MASW acquisition and processing, http://www.kgs.ku.edu/software/surfseis/masw.html

Lane, J.D., Ragland, W.S., Williams, R., and Penumadu, D., 2008, Use of MASW for geotechnical site characterization using corrected triaxial geophones: Proceeding of the SAGEEP 2008, Philadelphia, Pennsylvania, April 6-10

Long, M., and Donohue, S., 2007, In situ shear wave velocity from multi-channel analysis of surface waves (MASW) tests at eight Norwegian research sites, Canadian Geotechnical Journal, 44 (5): 533-544.

The Mathworks, Inc., 2007, MATLAB®, Version R2007a.

Miller, R.D., T.S. Anderson, J. Ivanov, J.C. Davis, R. Olea, C.B. Park, D.W. Steeples, M.L. Moran, and J. Xia, 2003, 3-D characterization of seismic properties at the Smart Weapons Test Range, YPG [Exp. Abs.]: Soc. Expl. Geophys., NSG 2.3

Miller, R.D., Xia, J., Park, C.B, Ivanov J., Geier, N., and Laflen, D., 1999, Using MASW to map bedrock in Olathe, Kansas: Kansas Geological Survey Open-file Report No. 99-9

Park, C.B., and R.D. Miller, 2003, MASW for shear wave velocity evaluation of soil before and after deep dynamic compaction operations: Kansas Geological Survey Open-file Report 2003-64.

Park, C.B., Miller, R.D., and Xia, J., 1999, Multi-channel analysis of surface waves, Geophysics, 64(3), 800-808

Park, C.B., Xia, J., and Miller, R.D., 1998b, Imaging dispersion curves of surface waves on multi-channel record: 68th Ann. Internat. Mtg., Soc. Expl. Geophys., Expanded Abstracts, 1377-1380.

Penumadu, D., and Park, C.B., 2005, Multi-channel analysis of surface wave method (MASW) for geotechnical site characterization., American Society of Civil Engineers Geotechnical Special Publication, Issue 130, 956-967.

Telford, W.M., Geldart, L.P. Sheriff, R.E. and Keys, D.A., 1976, Applied Geophysics, Cambridge University Press, Cambridge, 860pp.

Appendix

Tables

Table 2.1. Geophone parameter summary and wellness of curve fit.

	LRS-1000 (10 Hz Vertical Component)	L-28LBH (4.5 Hz Horizontal Component)
$f_n = \omega_n/2\pi$ (Hz)	9.984	4.959
ζ	0.6076	0.5057
Sensitivity (mV/(cm/s))	160.6	396.2
R^2	0.9773	0.9492

Figures

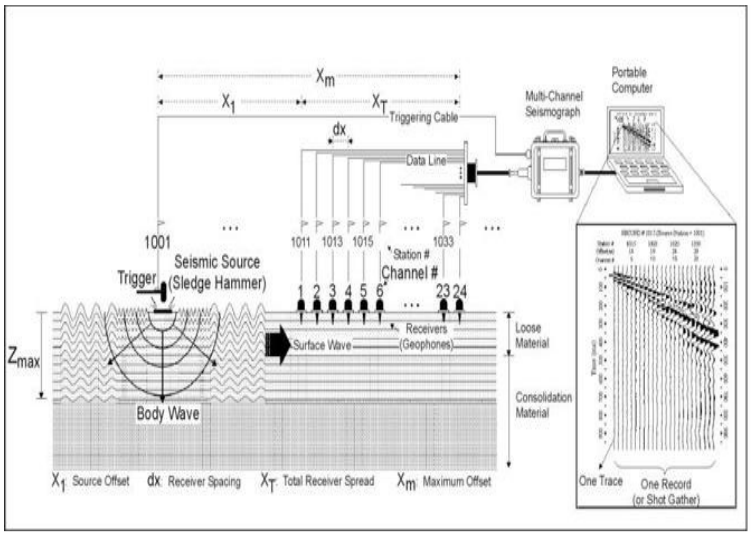

Figure 2.1. Typical MASW configuration (KGS 1998)

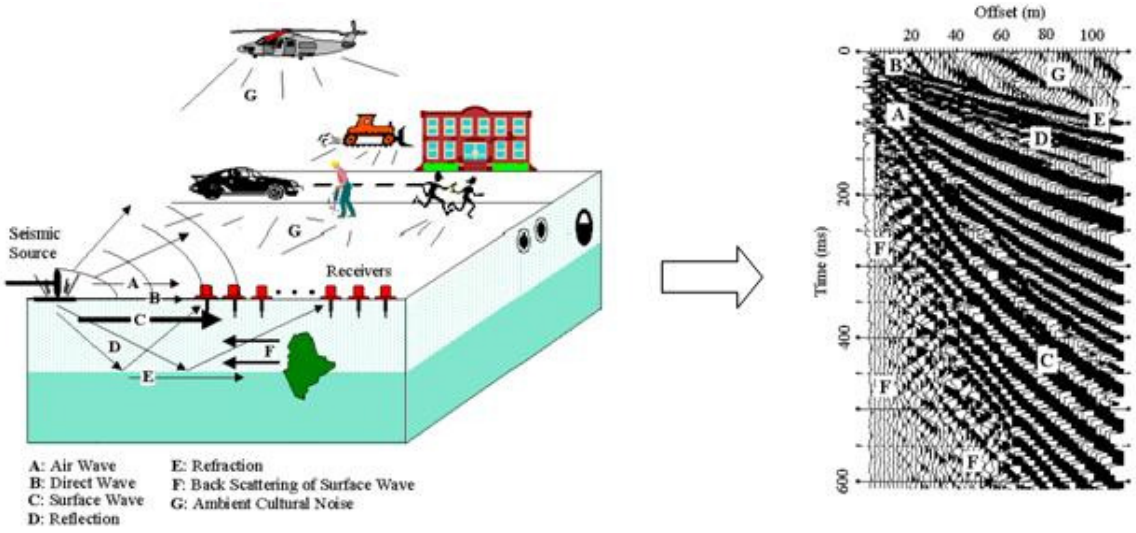

Figure 2.2. Background seismic waves and respective time series data (KGS 1998)

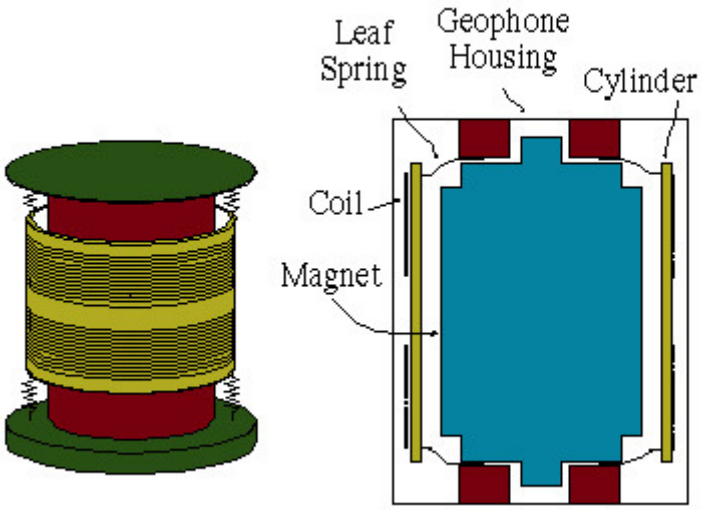

Figure 2.3. Geophone Schematic (Brincker 2005).

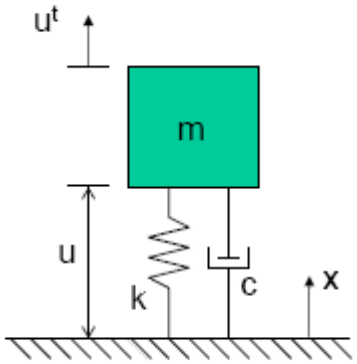

Figure 2.4. Geophone modeled as a single degree of freedom system.

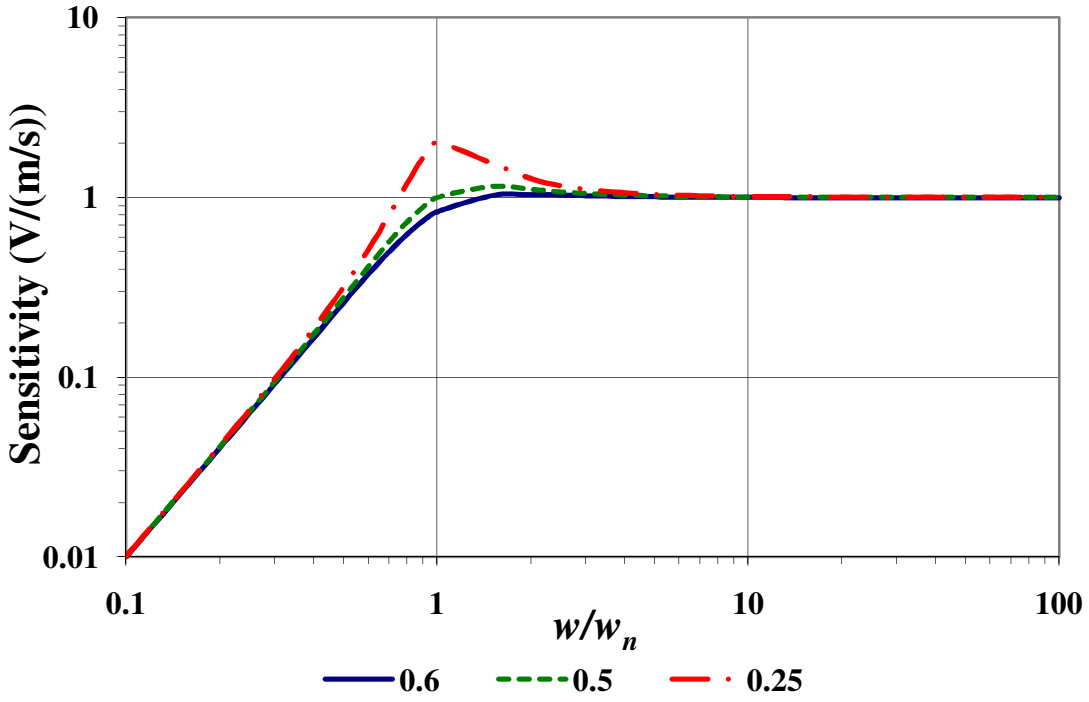

Figure 2.5. Geophone Sensitivity vs. the ratio of excitation frequency to geophone natural frequency for various damping ratios.

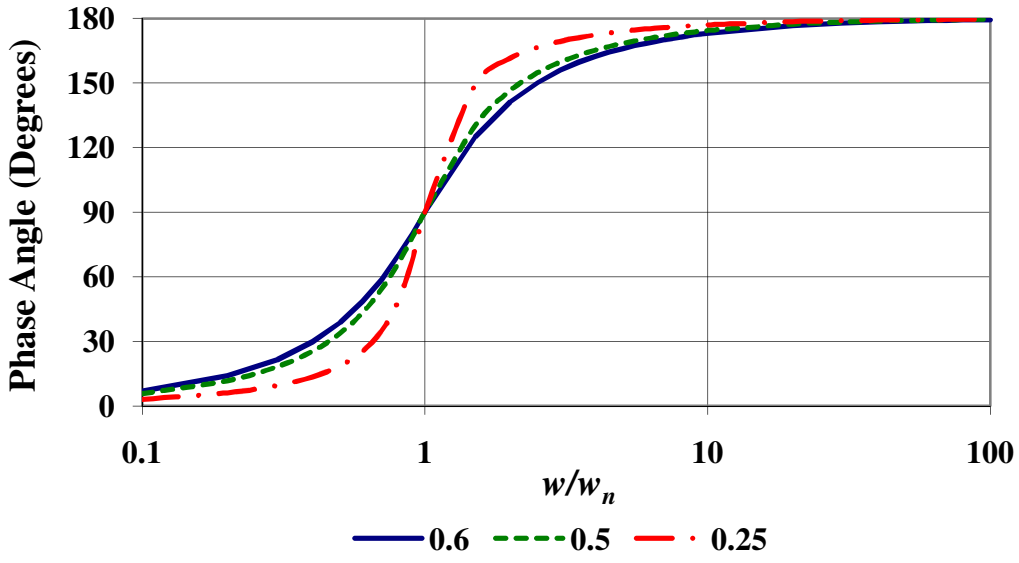

Figure 2.6. Geophone Sensitivity vs. the ratio of excitation frequency to geophone natural frequency for various damping ratios.

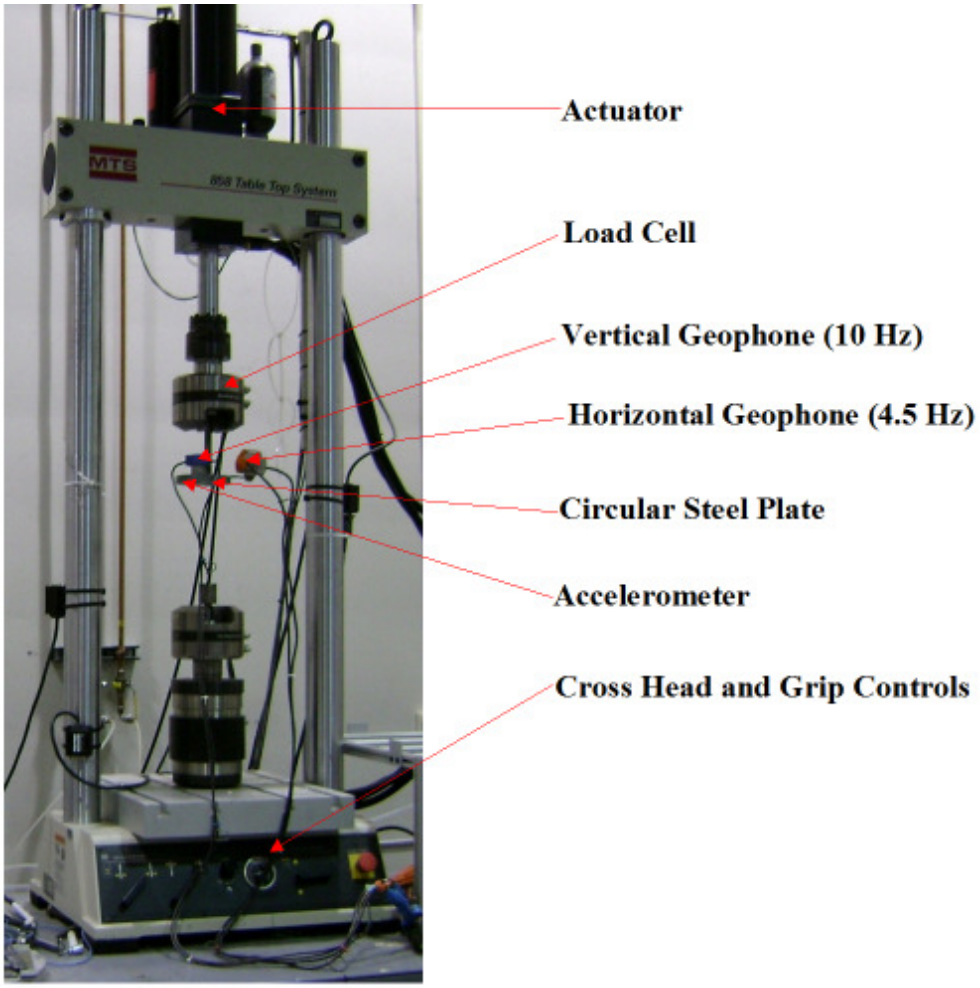

Figure 2.7. Mark Products RS-1000 10Hz vertical geophone (blue) and L-28LBH 4.5Hz horizontal geophone (orange) mounted on the MTS 858 servo-hydraulic device.

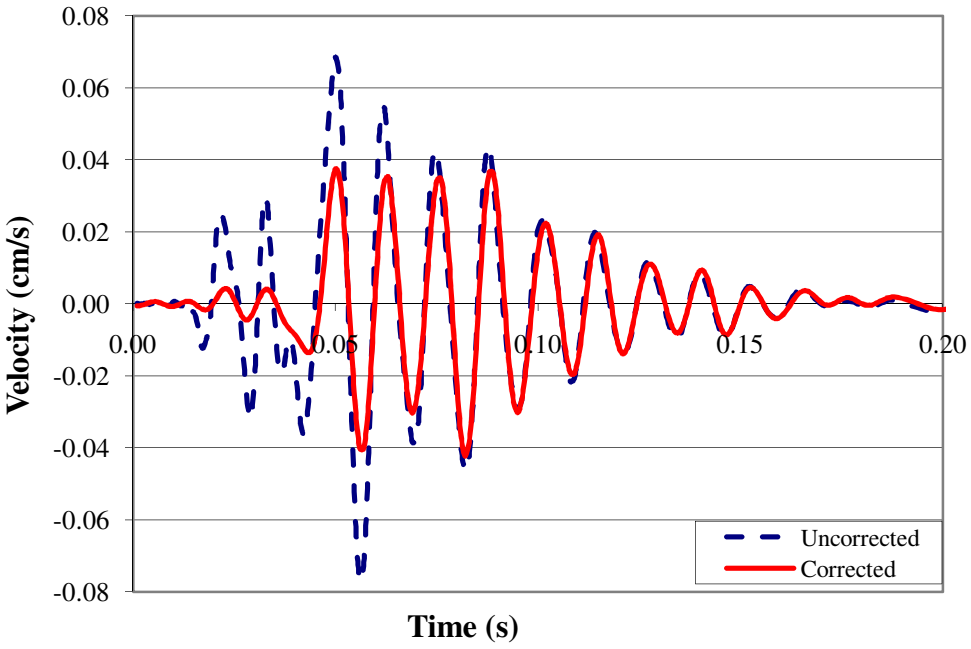

Figure 2.8. Seismic data before and after correction for the geophone response.

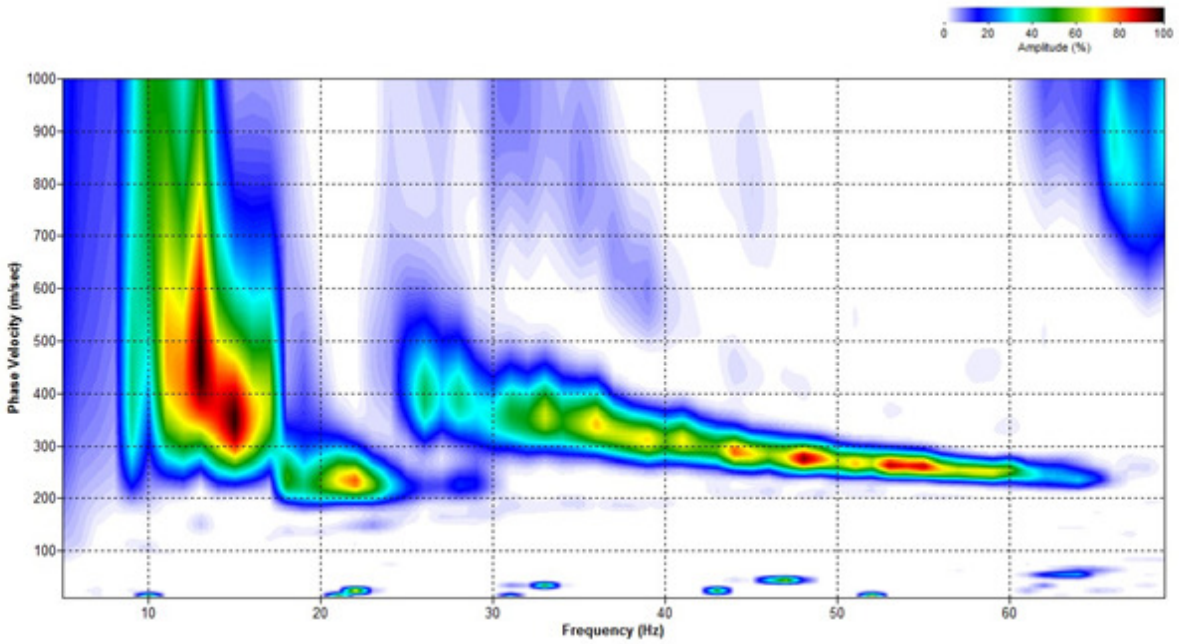

Figure 2.9. Uncorrected vertical component Rayleigh wave dispersion image.

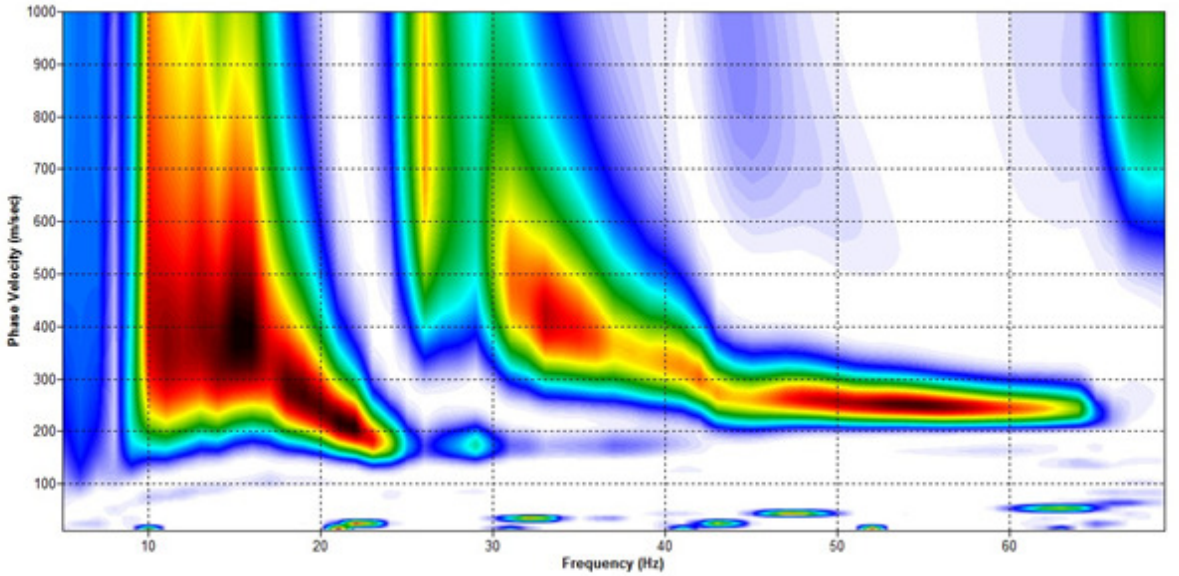

Figure 2.10. Corrected vertical component Rayleigh wave dispersion image.

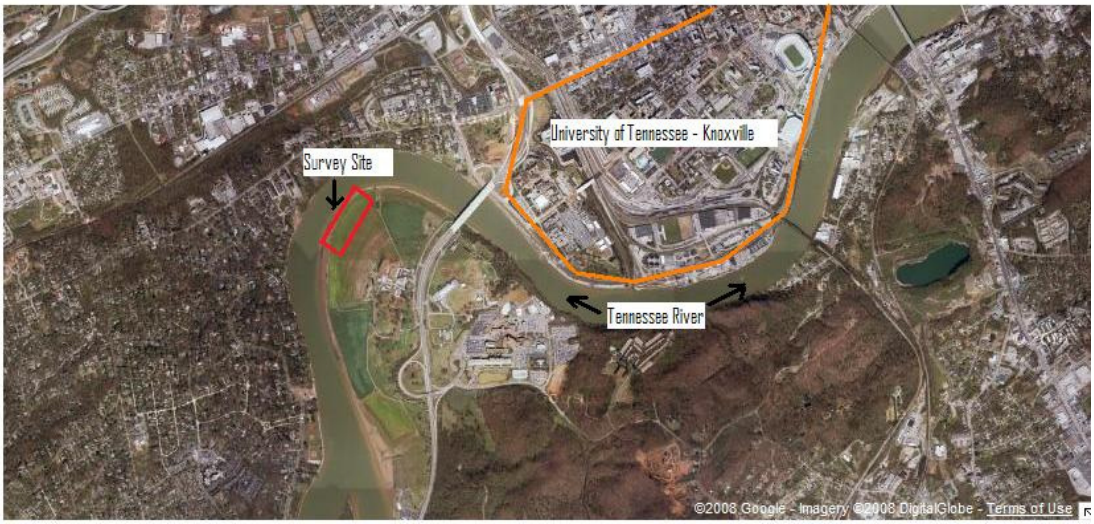

Figure 2.11. MASW site location.

Figure 2.12. Left – Source coupling, Right – Receiver coupling.

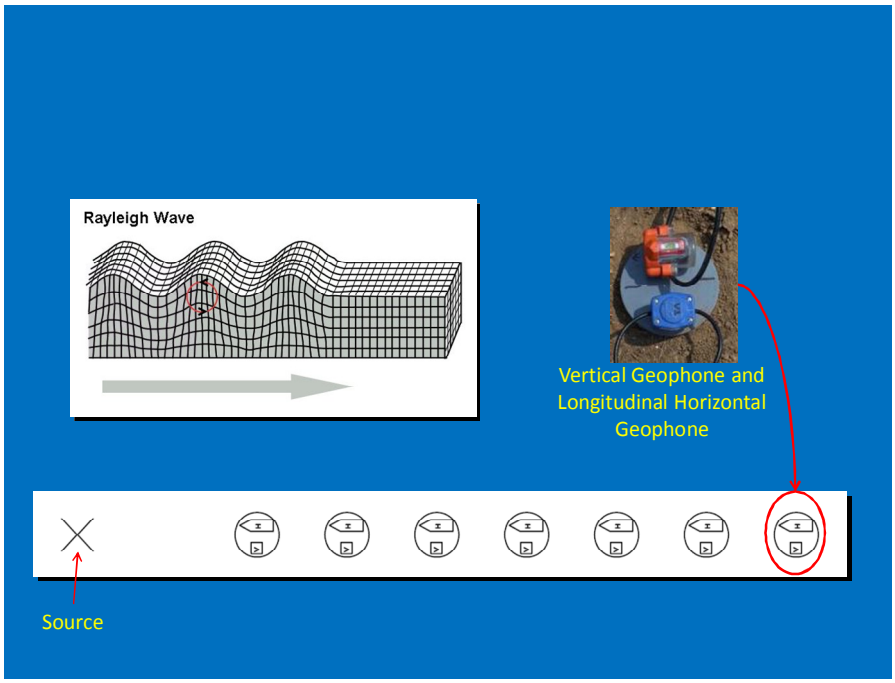

Figure 2.13. Measurement scheme of vertical and horizontal geophones for Rayleigh waves.

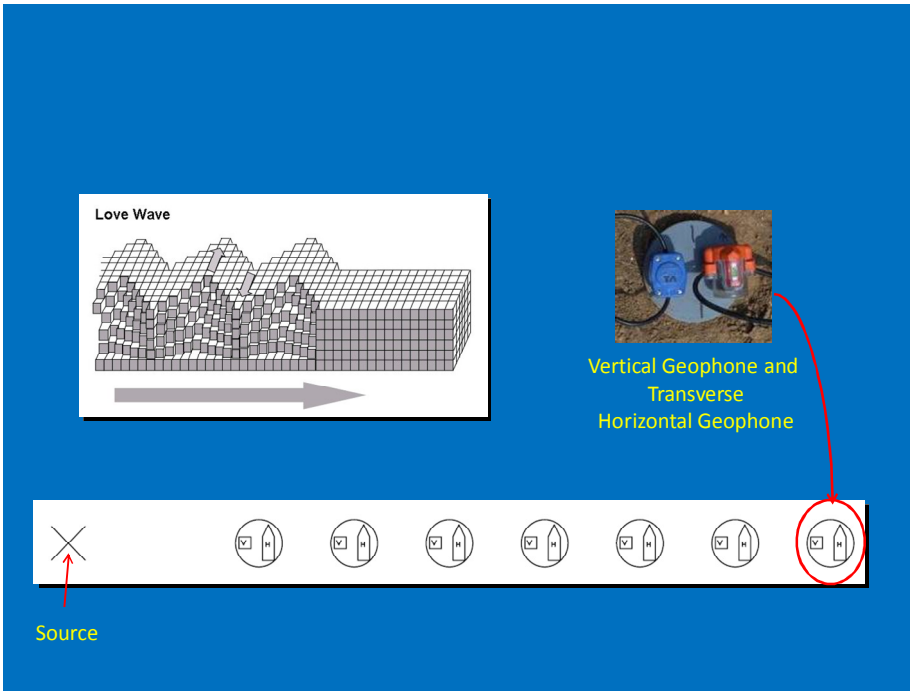

Figure 2.14. Measurement scheme of vertical and horizontal geophones for Love waves.

Figure 2.15. Top: Hammer and Plate source, Bottom left: 22.5kg Sand bag source, Bottom Center: Hammer and 45° wooden block, Bottom Right: ELECTRO-SEIS® Vibrator.

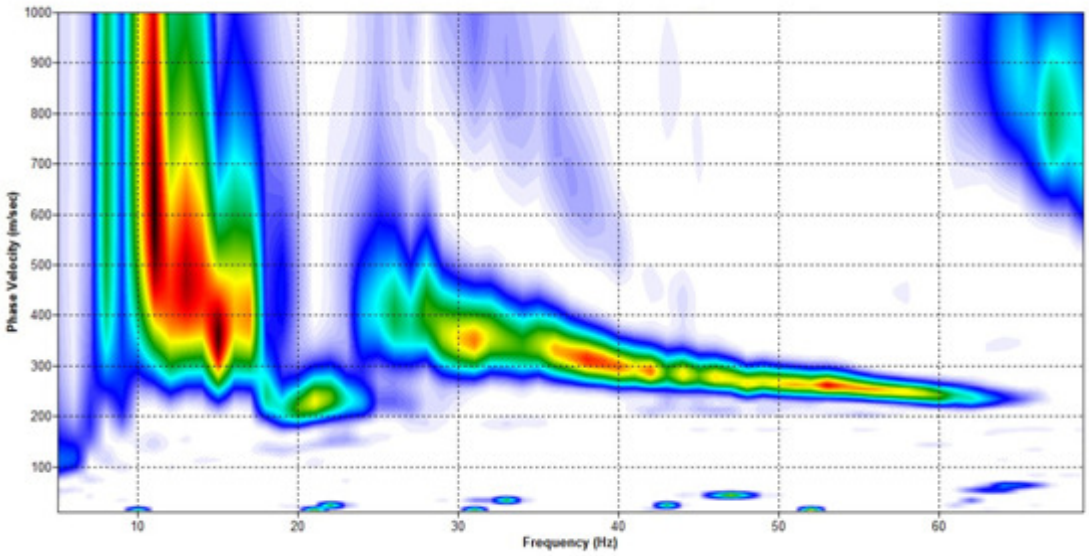

Figure 2.16. Vertical uncorrected Rayleigh wave dispersion image from 22.5kg bag of sand source.

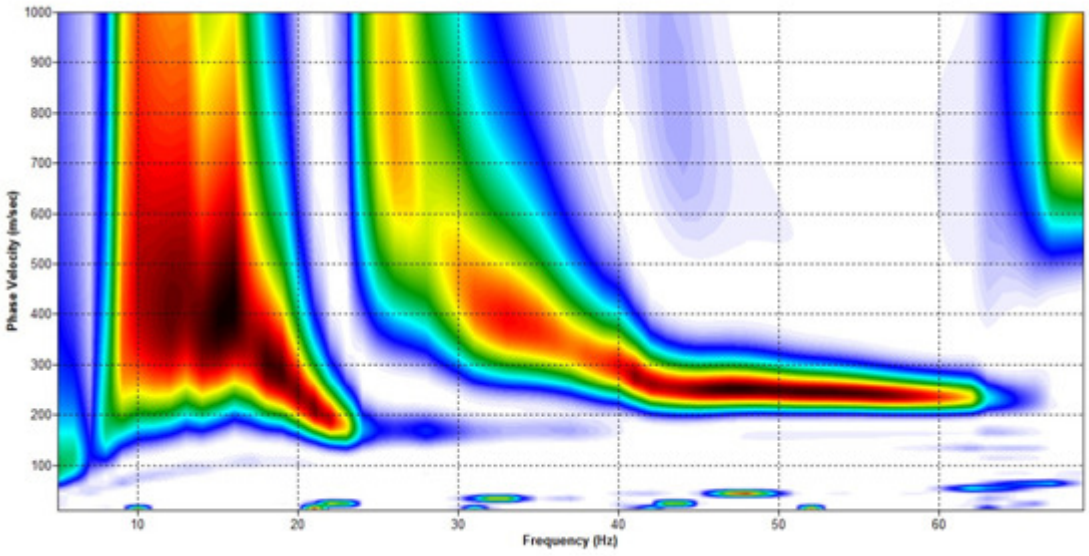

Figure 2.17. Vertical corrected Rayleigh wave dispersion image from 22.5kg bag of sand source.

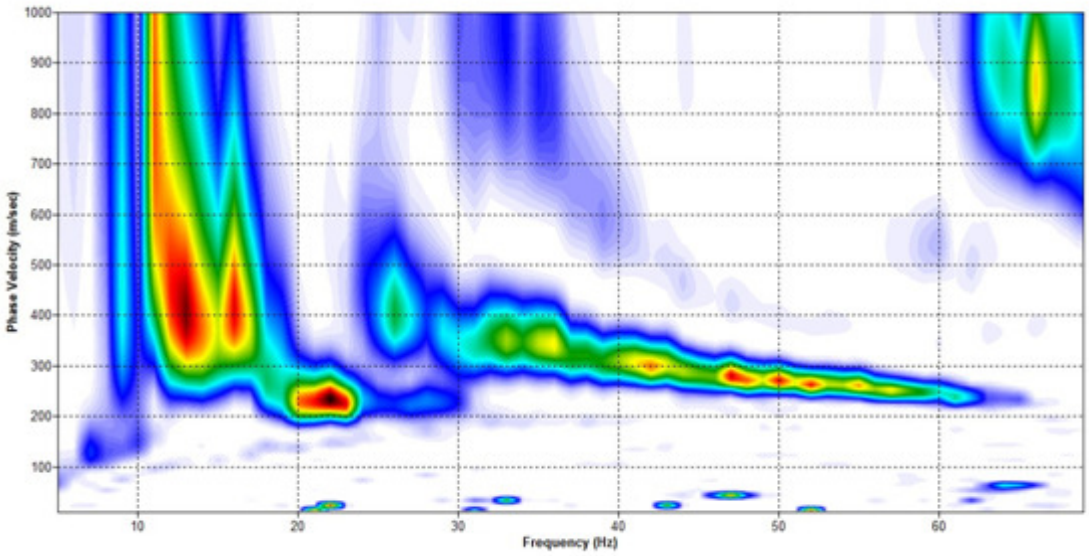

Figure 2.18. Vertical geophone uncorrected Rayleigh wave dispersion image from Hammer and Plate source.

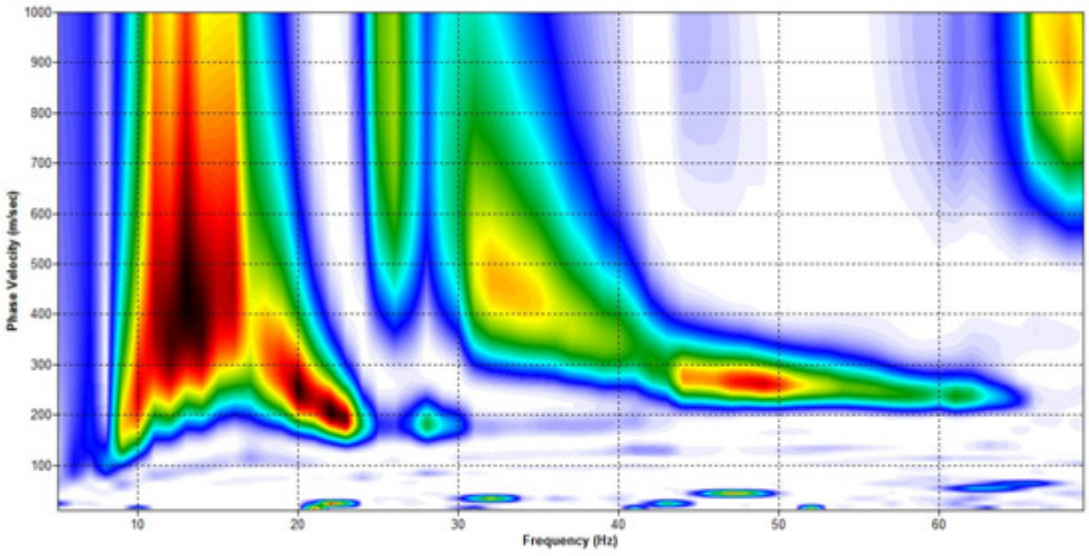

Figure 2.19. Vertical geophone response corrected Rayleigh wave dispersion image from Hammer and Plate source.

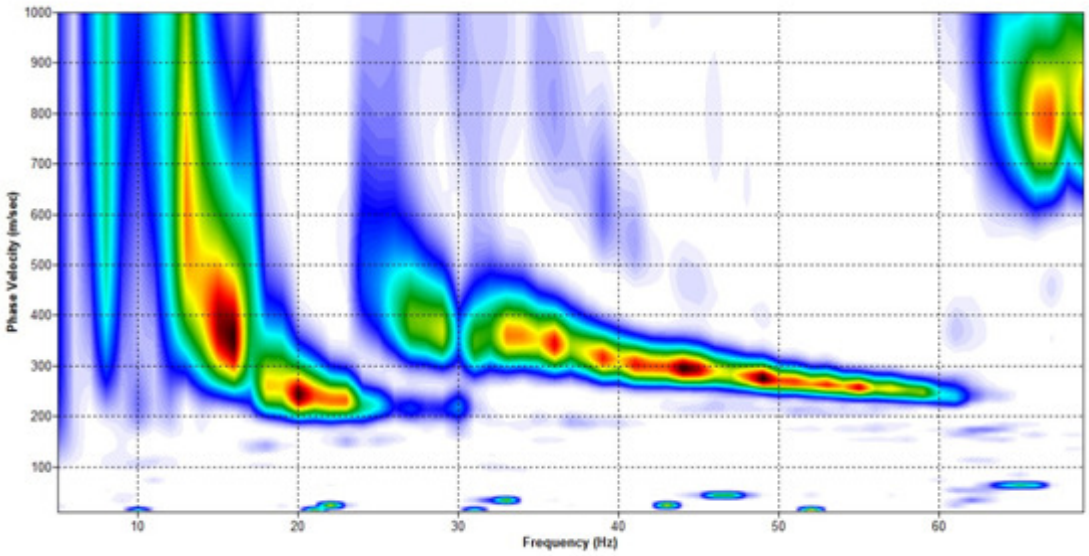

Figure 2.20. Vertical uncorrected Rayleigh wave dispersion image from Hammer and 45° wooden block source.

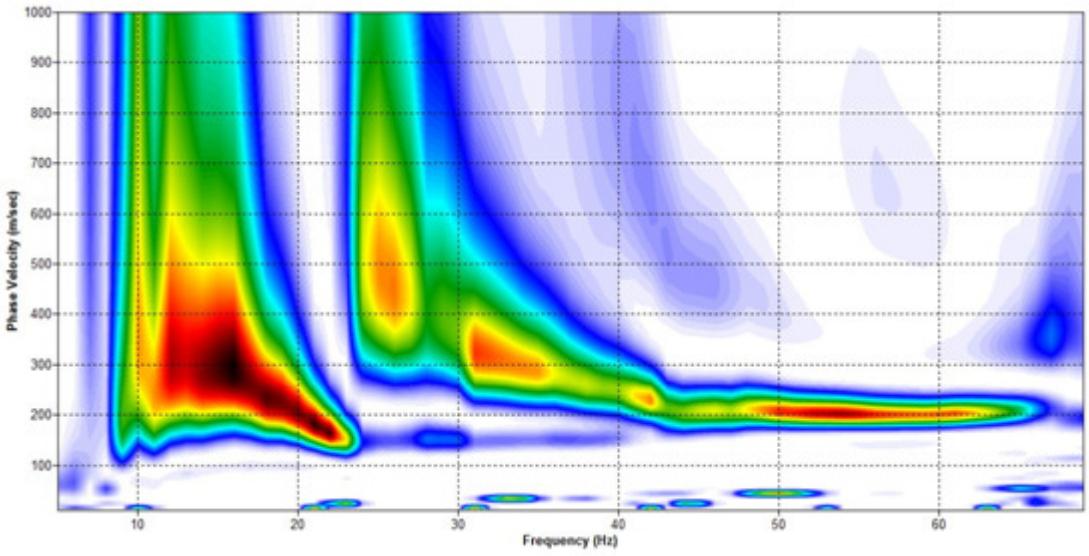

Figure 2.21. Vertical corrected Rayleigh wave dispersion image from Hammer and 45° wooden block source.

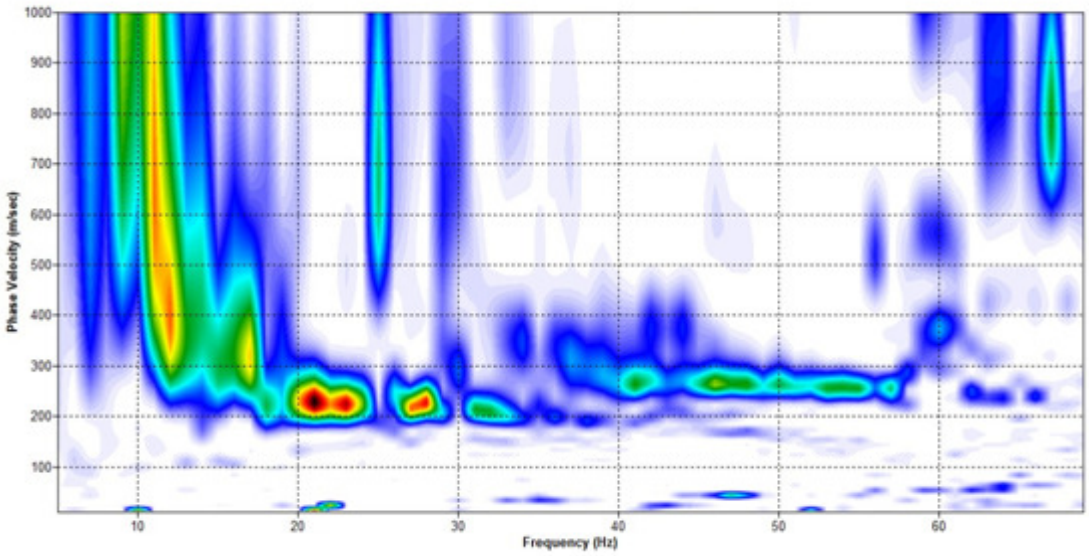

Figure 2.22. Vertical uncorrected Rayleigh wave dispersion image from ELECTRO-SEIS® vibrator source.

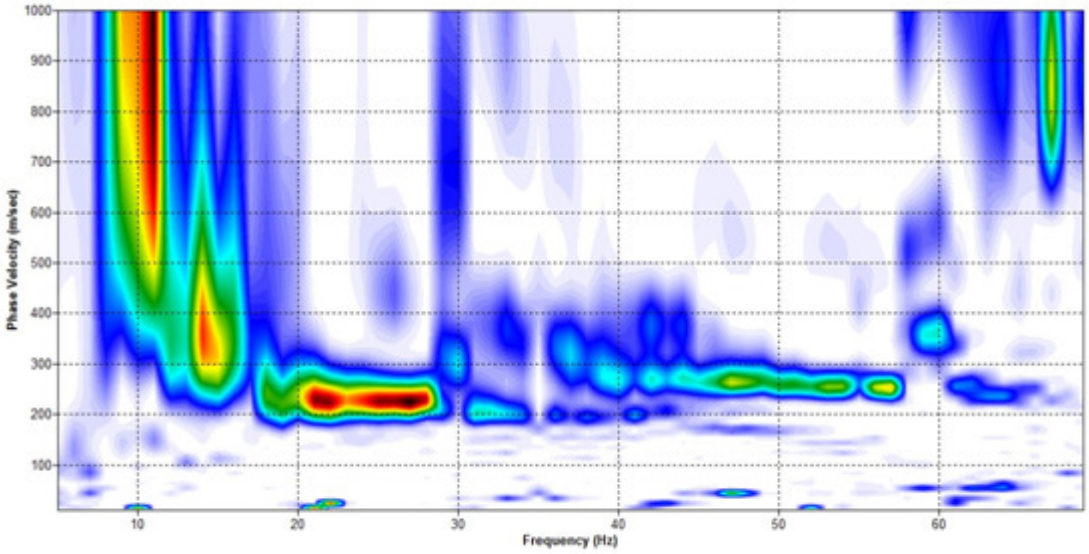

Figure 2.23. Vertical corrected Rayleigh wave dispersion image from ELECTRO-SEIS® vibrator source.

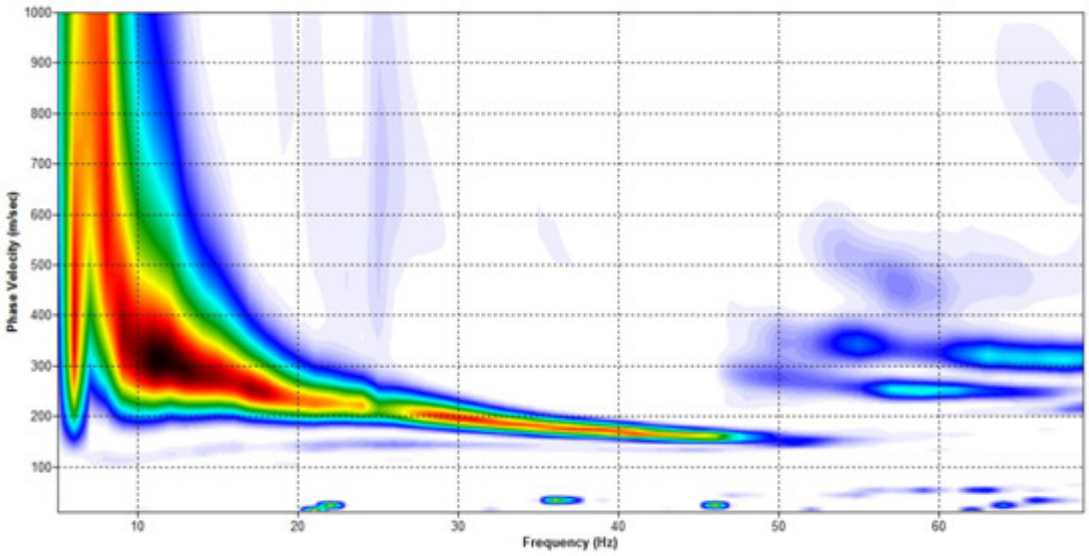

Figure 2.24. Transverse horizontal geophone uncorrected Love wave dispersion image from Hammer and 45° wooden block source.

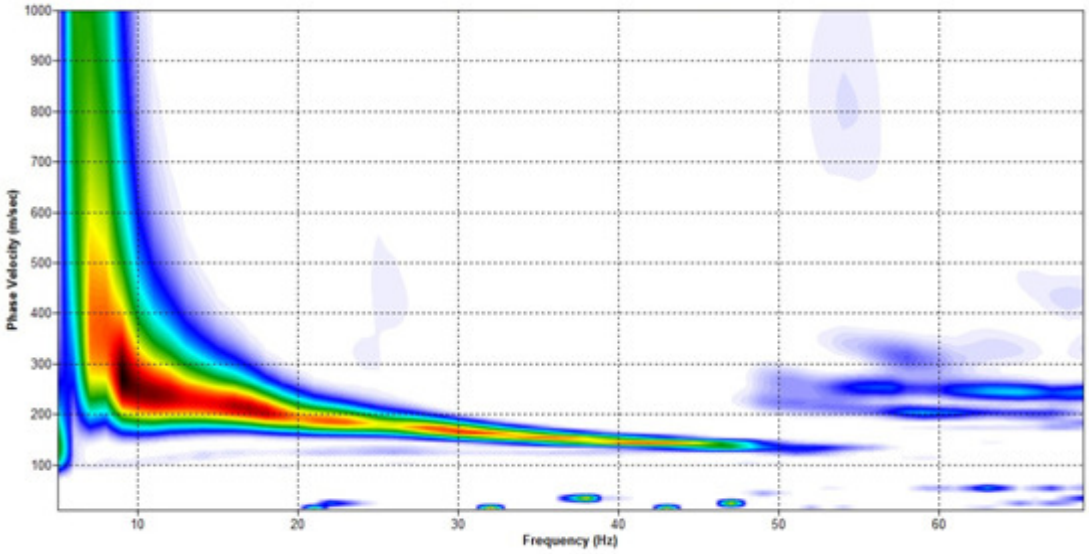

Figure 2.25. Transverse horizontal geophone corrected Love wave dispersion from Hammer and 45° wooden block source.

Chapter 3: Multi-Channel Analysis of Surface Waves (MASW) for Thin Soil above Bedrock for a Flood Plain Site of Tennessee River

My primary contributions to this paper include: (1) evaluation of the topic and development of the problem to study the optimum parameters for data collection at this specific site, (2) detailing the benefits of obtaining multi-axial surface wave data to compare geophone orientation with regard to the capture of Rayleigh Waves, (3) obtaining and interpretation of published literature, (4) performing all field experiments and subsequent data analysis and interpretation, and (5) performing the writing necessary for manuscript preparation.

Abstract

Locations where layers of soft sediment or soil overlay shallow bedrock are common in geotechnical engineering problems. Determination of the subsurface stratigraphy, shear wave velocity, and depth to bedrock using non-invasive methods in such settings is valuable where invasive methods are not possible or too expensive, such as at environmentally contaminated sites. The multi-channel analysis of surface waves (MASW) method was used to determine the shear wave velocities of soil layers on the flood plain of Tennessee River. Low frequency Rayleigh waves do not propagate below a cutoff frequency where bedrock is shallow. Fundamental mode Rayleigh wave dispersion curves were determined based on MASW survey data and inverted using SurfSeis software from the Kansas Geological Survey. The inversion results calculated in SurfSeis did not discover bedrock based on the dispersion curves. A misfit of the dispersion curves at frequencies below ~10 Hz was revealed by forward modeling using the Computer Programs in Seismology (CPS) software from the University of St. Louis, and a Rayleigh-Lamb model instead of classical Rayleigh wave theory. Inversions based on the CPS

Rayleigh-Lamb model were not performed due to the uncertainty in the interpretation of the fundamental mode Rayleigh wave dispersion curve at the lowest observed frequencies.

Introduction

The multi-channel analysis of surface waves (MASW) method (Park et al., 1999) has emerged as a valuable technique for non-invasive seismic testing to evaluate shear-wave velocity or stiffness of the ground and subsurface for geotechnical site characterization (Penumadu and Park, 2005; Long and Donahue, 2007). The method involves the analyses of the phase velocity dispersion of certain seismic surface waves (fundamental-mode Rayleigh waves) propagating horizontally along the ground surface. Shear wave velocity information is typically presented in 1-D (depth) or 2-D (depth and surface location) format. The fundamental framework of the MASW method is based on the multi-channel recording approach long used in seismic exploration surveys (Telford et al., 1976) that can discriminate useful seismic signals from noise.

Numerous case studies of MASW applications for different purposes exist, including geophysical, geological, environmental, and geotechnical engineering projects. Miller et al. (1999) successfully applied the MASW technique to map weak spots in bedrock. Ivanov et al. (2006) used MASW to delineate a shallow fault zone and dipping bedrock strata using MASW. A 3-D shear velocity mapping was also accomplished using the MASW method at a military weapon test site in Arizona (Miller et al., 2003). Ivanov et al. (2003) and Park et al. (1998b) used the method to detect underground anomalies. MASW was also used to evaluate the effectiveness of a compaction operation conducted as a soil remediation tool at a construction site (Park et al., 2003).

The goal of the present study is to determine shear wave velocities at a site located on the flood plain of the Tennessee River (Figure 3.1, all tables and figures are located in the Chapter 3 Appendix). The flood plain is expected to have soft, low velocity soil layers over high velocity bedrock, which is Knox dolomite (Cattermole, 1958). The S-wave velocity of Knox dolomite is not known at this particular location, but Christensen and Szymanski (1991) sampled it in East Tennessee near the town of Thorn Hill ~30 km away, and conducted laboratory studies of its seismic properties. They reported P-wave velocities at a range of confining pressures, but not S-wave velocities. At low (10 MPa) confining pressure they measured Vp = 6120 m/s. If we assume that Poisson's ratio for the dolomite is 0.25, then Vs = 3530 m/s. Thus it is reasonable to expect that Vs on average can be estimated to be ~3,000 m/s in bedrock.

There is a well-known effect where Rayleigh-Lamb waves (Rayleigh waves guided in layers) do not propagate at low frequencies, from DC to a cut-off frequency, in elastic layers that are clamped on one side (Worden, 2001). On the flood plain, S-wave velocities in the soil layers are perhaps 10 times slower than the S-wave velocity in the underlying Knox dolomite. In this situation, the bedrock layer is effectively rigid, and the wave energy travels in a wave guide formed by the layers between bedrock and the free surface. Theoretical dispersion curves for such wave guides, illustrated in Figures 3.2 and 3.3, were published by Vorovich and Babeshko (1979). Here, field experiments were conducted to show the limitation of Rayleigh wave propagation and S-wave velocity measurements using the MASW method in this particular subsurface environment.

Survey Setup

The seismic survey was conducted using a Geometrics, Inc. model RX-48 seismograph and 48 geophones. The 48 geophones consisted of 24 verticals and 24 horizontals, with one each vertical and horizontal geophone mounted together on a circular steel plate for biaxial recording. Several seismic sources were tested in order to determine which one yielded the best dispersion images.

Good coupling between the geophone and the soil is an important consideration for obtaining the best possible data. For this reason, geophones commonly have a spike on the bottom, which is intended to be set firmly into the soil. The geophones used here lacked a spike, because they were also intended for use on hard pavements, and in any case the spike does not always guarantee a good connection to the soil. Instead of using a spike and setting the geophone on the surface, 0.2 meter of topsoil was removed and both the geophones and seismic sources were deployed in shallow holes (Figure 3.4). Biaxial geophones were spaced at 1 m intervals for a total array length of 24 m. Four different MASW data sets were collected, one with the source-offset distance fixed at 5 m while both source and geophones were moved, and three others in which the source position was fixed and only the geophones were moved. In theory, Rayleigh waves can be detected utilizing vertically oriented geophones and horizontal geophones oriented radially. The survey setup for Rayleigh wave dispersion measurements is illustrated in Figure 3.5.

Comparison of Different Seismic Sources

Four different seismic sources, shown in Figure 3.6 were compared in this study: (1) sledge hammer and aluminum plate lying flat on the ground; (2) 22.5 kilogram bag of sand dropped from a height of 1 m; (3) sledge hammer and 45° wooden block to generate both Rayleigh and Love waves from the same hit; and (4) ELECTRO-SEIS® vibrator. Illustrative dispersion images from the four sources are presented in Figures 3.7 through 3.10.

In principle, the phase velocity at any given frequency depends only on the shear wave velocity structure associated with the underlying soil, not on the properties of the seismic source. For this reason, the dispersion images should be similar for all four sources in the test. There are, however, possible differences in the amplitude spectra of the different sources, and in the excitation of higher modes that must be taken into account. The two sledge hammer sources (Figures 3.7 and 3.9) yield almost the same dispersion images, where fundamental mode and first higher mode dispersion curves can be interpreted. Comparison of all four Figures 3.7 – 3.10 suggests upon first glance that the ELECTRO-SEIS® source produced the most continuous fundamental mode Rayleigh wave dispersion curve, but the situation is not simple. Close comparison of Figure 3.9 and 3.10 in the frequency range 40 – 60 Hz suggests that the ELECTRO-SEIS® image (Fig. 3.10) shows fundamental mode from 40 – 45 Hz, but first higher mode above 45 Hz. If one were not to consider data using the sledge hammer data as the seismic energy source, it seems likely that the ELECTRO-SEIS® image would have been misinterpreted to consist of fundamental mode energy in this frequency range. The 22.5 kg bag of sand source led to a dispersion image (Figure 3.8) that is similar at most frequencies to the sledge hammer and 45° wooden block image (Figure 3.9). Both of these sources seem better than the hammer

and aluminum plate (Figure 3.7) at the lowest frequencies. Even though the ELECTRO-SEIS® source produced the best continuous fundamental mode Rayleigh wave dispersion, it is cumbersome and impractical for MASW. Thus, the simple hammer and 45° wooden block out performed all of the other sources at most frequencies.

Source Offset Distance

Data were collected at different offset distances from 1 m to 28 m. As with the kind of source used, the phase velocity at any given frequency should depends only on Vs in the underlying soil, not on offset distance. The purpose of these experiments was to determine whether there is an optimum offset, in terms of the dispersion images inferred. The offset experiments were performed using the sledge hammer and 45° wooden block seismic source. Vertical and horizontal/radial geophones were used. The 1 m offset produced the dispersion image shown in Figure 3.11. For comparison, Figure 3.9 shows the dispersion image obtained for 5 m offset. The 5 m offset works better than 1 m, especially at lower frequencies. This is result is consistent with the conclusion by Park et al. (1999) that there is a near-field effect that results in a lack of phase coherency at lower frequencies.

The results for greater offsets, from 5 m, 16.5 m, and 28 m are shown in Figures 3.9, 3.12, and 3.13, respectively, where the source was the 22.5 kg bag of sand. In this instance, the shortest offset tested (5 m) worked best, probably due to attenuation of the seismic waves and lower signal-to-noise ratio at the longer offsets. Zhang et al. (2004) proposed the following equation for optimum offset (A):

$$A = \frac{\lambda_{\max} \; c_{R\min}}{4\,\Delta \; c_{\mathrm{R}}}, \qquad (1)$$

where $\lambda_{\max}$, $c_{R\min}$, and Δc_{R} are the longest wavelength, the minimum phase velocity of the Rayleigh waves, and the difference between maximum and minimum phase velocity, respectively. For our site, $\lambda_{\max}$ =≈ (450 m/s/10 Hz) = 45 m, $c_{R\min}$= 150 m/s, and Δc_{R}= (450 m/s – 150 m/s) = 300 m/s. Thus, the optimum offset according to the proposal by Zhang et al. (2004) would be 5.6 m, which is consistent with the 5 m observed here.

Geophone Orientation

Rayleigh waves are associated with elliptical retrograde particle motions. The ellipticity *e* = H/V, where H is the horizontal axis of the ellipse and V is the vertical axis, is commonly in the range 0.7 – 0.8 (Malischewsky and Scherbaum, 2004). In stratified materials *e* is dispersed, varying with frequency and mode number, as well as G and ν in the strata, where G and ν are shear modulus and Poisson's ratio, respectively. In general, either vertical component geophones or horizontals can be used to determine the dispersion of the fundamental mode Rayleigh waves, although vertical geophones might be better for this purpose, because V is commonly greater than H. Dispersion images are presented in Figures 3.8 and 3.9 for the vertical component, and in Figure 3.14 for the radial component. Comparison of 3.8 and 3.9 versus 3.14 confirms that the vertical works better than the horizontal component for the fundamental mode, especially at lower frequencies.

MASW Survey

The survey setup consisted of 24 biaxial geophones having vertical and horizontal (radial) components, spaced at 1 m intervals (Figure 3.4). Commonly, the MASW technique

involves moving the source and geophones together in a roll along pattern (Dobrin and Savit, 1988), which in this case advances everything in 1 meter increments from one source point to the next. For the MASW analysis, subsets of 12 geophones were extracted from the 24 geophone array, yielding 13 data records with 12 geophones in each record. The 13 data records span an MASW profile length of 13 m. The seismic source was a sledge hammer striking a 45° wooden block, located at 5 m offset distance. The data from the first source point are shown in Figure 3.16 as an example.

An interpreted Rayleigh wave dispersion image computed from the data vertical geophone data in Figure 3.16 is presented in Figure 3.17. The figure also shows the fundamental mode Rayleigh wave dispersion curve (white squares) interpreted from the dispersion image. The points on this dispersion curve were utilized for shear wave velocity inversion in SurfSeis. This process was repeated 13 times, once for each source point. Shear wave velocities resulting from the 13 individual inversions are shown in the columns of Table 1. It is assumed in the SurfSeis inversion that Vp/Vs = 2.45, corresponding to $\nu = 0.4$, and that density is 2.0 g/cm^3 in every layer.

The accuracy of the SurfSeis inversion was verified by forward modeling using programs from the Computer Programs in Seismology (CPS) software suite (Hermann, 1996). The solid black curves in Figure 3.17 are the fundamental and first higher mode dispersion curves for the subsurface layers in the first column of Table 1. It can be seen that the CPS calculations exactly match the data points (white squares) input to the inversion process, which verifies that the SurfSeis inversion worked as expected. The forward modeling was extended outside the range of the fundamental mode data, and to the first higher mode, which was not used in the SurfSeis

inversion. The figure also shows that the first higher mode dispersion is also explained, in part, by the same subsurface layers, even though no first higher mode data was input to the inversion process. The solid black curve that represents the predicted first higher mode passes through the energy (red color) that represents the observed first higher mode in the frequency range 40 – 65 Hz.

Rayleigh-Lamb Model

The CPS calculations (solid black lines in Figure 3.17) also reveal certain short comings in the inversion results. Principal among these is the misfit at the lowest frequencies, below ~10 Hz. The dispersion image shows that no Rayleigh wave energy was propagating at frequencies lower than 10 Hz for phase velocities slower than 1,000 m/s, the upper limit of the figure. This portion of the figure is blank, devoid of seismic energy. In contrast, the SurfSeis inversion is based on the usual model for Rayleigh waves, i.e. layers above a half-space, and the half-space is the bottom layer shown in Table 1. In this model, the fundamental mode dispersion curve extends to low frequencies at phase velocities in the 500 – 600 m/s range, as depicted by the black line in Figure 3.17, but no such Rayleigh wave was observed.

The soil at the test site is underlain by bedrock comprised of Knox dolomite (Cattermole, 1958), and seismic velocities in these rocks are ~10 times greater than in the soil. The bedrock was not found by the SurfSeis inversion, and therefore does not appear in Table 1. The strong contrast between elastic properties in the soil and bedrock points to the need for a different model, a Rayleigh-Lamb model (Worden, 2001) for the surface waves, instead of the classical Rayleigh wave model. In the Rayleigh-Lamb model, the soil layers form a waveguide,

which is bounded on the top by the free surface and on the bottom by the dolomite, which is almost rigid in comparison to the soil. The influence of the Knox dolomite bedrock is illustrated by the dashed lines in Figure 3.17, where the basal half-space from the SurfSeis model has been replaced by Knox dolomite instead.

Replacing the half-space of the Rayleigh wave inversion with an almost rigid basal layer to represent bedrock did not change the results in the portion of the dispersion image where the dispersion data was used for inversion. (The dashed lines and the solid lines both go through the white squares in Figure 3.17.) The presence of stiff basement rocks explains the absence of Rayleigh wave energy at frequencies lower than ~10 Hz, but additional work is needed to fully account for everything in the dispersion image.

MASW Profile: Results from SurfSeis

The 13 individual dispersion data sets obtained from the 13 MASW seismic data records (e.g. Fig. 3.16) were inverted using SurfSeis to produce the 2-D shear velocity profile presented in Figure 3.18. The 1-D inversion results are summarized in Table 3.1 as a function of location and depth. The location on the ground surface is taken to be the mid-point of the 12 geophones used for the data record. Only fundamental mode dispersion data (e.g. white squares in Fig. 3.17) were used for the inversions. As SurfSeis was used for the inversions, the result (Fig. 3.18 and Table 1) is based on the classical Rayleigh wave model, where high velocity bedrock is not explicitly included. In principle, the Rayleigh wave model can also find bedrock, but bedrock does not appear in the results (Table 1). The highest velocity found in the inversions was ~700 m/s, which is characteristic of soil, not hard rock.

Alternately, the inversions could be based on the Rayleigh-Lamb model, where the soil is assumed from the outset to be underlain by bedrock. Importantly, the depth to bedrock is an unknown in the Rayleigh-Lamb model; only the existence of bedrock, not the depth to bedrock, is assumed.

Number of Layers in the Model

The inversion results obtained here (Fig. 3.19 and Table 1) were based on an assumption that the soil contains 10 layers. It is not obvious, however, what the appropriate number of soil layers should be. This question was addressed in a numerical experiment, where the dispersion data were inverted using different numbers of layers ranging from 1 layer to 10 layers. The results are summarized on Figures 3.20 and 3.21. It can be seen in the figures that the results from a 5-6 layer inversion are close to the 10 layer inversion.

Conclusions

1. Bedrock was not detected by inversion of the fundamental mode Rayleigh wave dispersion data in SurfSeis.

2. Inversion of the dispersion curves in this situation may be improved by using a different model, with the soil layers forming a wave guide that is clamped on the bottom by semi-rigid bedrock (Rayleigh-Lamb waves) instead of classical Rayleigh waves.
3. The ELECTRO-SEIS® vibrator produced the best dispersion image for the fundamental mode. The vibrator, however, was less effective at exciting higher mode Rayleigh waves

and was cumbersome to use in the field. The best source overall was the simple sledge hammer and wooden block.

4. Concerning the optimum source offset distance, the equation proposed by Zhang et al. (2004) is useful in the case of soil over shallow bedrock (Rayleigh-Lamb waves), but the depth to bedrock is the principal variable controlling the optimum offset.

5. Rayleigh wave dispersion can be measured using either vertical or horizontal (radial) geophones. The vertical data are somewhat better than the horizontal, and there is little to be gained by using both.

6. Fundamental mode Rayleigh wave dispersion data can be explained using a relatively small number of soil layers. The resolution of the MASW technique is not improved by increasing the number of layers in the soil used the inversion process.

References

Cattermole, J.M. 1958, Geology of the Knoxville Quadrangle, Tennessee, Geologic Quadrangle Map GQ-115, U.S. Geological Survey

Christensen, N.I. and Szymanski, D.L., 1991, Seismic properties and the origin of reflectivity from a classic Paleozoic sedimentary sequence, Valley and Ridge province, southern Appalachians, GSA Bull. 103, 277-289.

Dobrin, M.B, and Savit, C.H., 1988, Introduction to Geophysical Prospecting, McGraw-Hill, New York, 867 pp.

Hermann, R. B., 1996, Computer Programs in Seismology (CPS) [computer program], Ver. 3.30, unpublished software distributed by Saint Louis University.

Ivanov, J., Miller, R.D., Lacombe, P., Johnson, C.D., and Lane Jr., J.W., 2006, Delineating a shallow fault zone and dipping bedrock strata using multi-channel analysis of surface waves with a land streamer, Geophysics 71(5), A39-A42

Ivanov, J., R.D. Miller, C.B. Park, and N. Ryden, 2003, Seismic search for underground anomalies, [Exp. Abs.]: Soc. Expl. Geophys., NSG3.2

Kansas Geological Survey (KGS), 2006, SurfSeis [computer software], Ver. 2.05

Kansas Geological Survey (KGS), 1998, Introduction to MASW acquisition and processing, http://www.kgs.ku.edu/software/surfseis/masw.html

Long, M., and Donohue, S., 2007, In situ shear wave velocity from multi-channel analysis of surface waves (MASW) tests at eight Norwegian research sites, Canadian Geotechnical Journal, 44 (5): 533-544.

Malischewsky, P.G., and Scherbaum, F., 2004, Love's formula and H/V-ratio (ellipticity) of Rayleigh waves, Wave Motion, 40:57-67

Miller, R.D., Anderson T.S., Ivanov, J., Davis, J.C., Olea, R., Park, C.B., Steeples, D.W., Moran, M.L., and Xia, J., 2003, 3-D characterization of seismic properties at the Smart Weapons Test Range, YPG [Exp. Abs.]: Soc. Expl. Geophys., NSG 2.3

Miller, R.D., Xia, J., Park, C.B, Ivanov J., Geier, N., and Laflen, D., 1999, Using MASW to map bedrock in Olathe, Kansas: Kansas Geological Survey Open-file Report No. 99-9

Park, C.B., and R.D. Miller, 2003, MASW for shear wave velocity evaluation of soil before and after deep dynamic compaction operations: Kansas Geological Survey Open-file Report 2003-64.

Park, C.B., Miller, R.D., and Xia, J., 1999, "Multi-channel analysis of surface waves," Geophysics, 64(3), 800-808

Park, C.B., Xia, J., and Miller, R.D., 1998b, Imaging dispersion curves of surface waves on multi-channel record: 68th Ann. Internat. Mtg., Soc. Expl. Geophys., Expanded Abstracts, 1377-1380.

Penumadu, D., and Park, C.B., 2005, Multi-channel analysis of surface wave method (MASW) for geotechnical site characterization. American Society of Civil Engineers Geotechnical Special Publication, Issue 130, 956-967.

Telford, W.M., Geldart, L.P. Sheriff, R.E. and Keys, D.A. 1976, Applied Geophysics, Cambridge University Press, Cambridge, 860pp.

Vorovich, V.V., and Babeshko, V.A., 1979, Mixed dynamic problems of elasticity for non-classical domains, Moscow, Nauka, 320 pp. (in Russian)

Worden, K., 2001, Rayleigh and Lamb Waves – Basic Principles, Strain, Vol. 37, No.4, 167-172.

Zhang, S.X., Chan, L.S., and Xia, J., 2004, The selection of field acquisition parameters for dispersion images from multichannel Surface-wave data, Pure and Applied Geophysics, 161:185-201

Appendix

Tables

Table 3.1. Shear velocities (m/s) as a function of source point and depth for a 10 layer inversion. The basal layer is a half-space.

	Source Point												
Depth (m)	**1**	**2**	**3**	**4**	**5**	**6**	**7**	**8**	**9**	**10**	**11**	**12**	**13**
-0.27	214	191	210	181	182	205	187	173	183	157	183	219	197
-0.61	232	222	224	209	243	219	208	232	226	229	225	225	232
-1.03	206	223	216	214	270	228	211	257	242	277	239	230	258
-1.56	126	167	177	173	203	221	186	192	208	221	194	199	264
-2.23	109	107	132	115	104	188	138	102	126	97	108	135	223
-3.05	209	180	165	167	180	145	145	179	151	168	157	142	153
-4.09	305	281	262	266	295	194	236	292	237	269	280	277	189
-5.38	356	337	326	327	318	323	323	329	312	317	332	363	275
-7.00	352	348	347	357	309	414	384	346	383	358	351	374	375
-9.02	345	372	367	401	366	470	429	401	443	431	380	350	454
-11.28	641	646	632	640	689	684	629	666	643	683	662	610	728

Figures

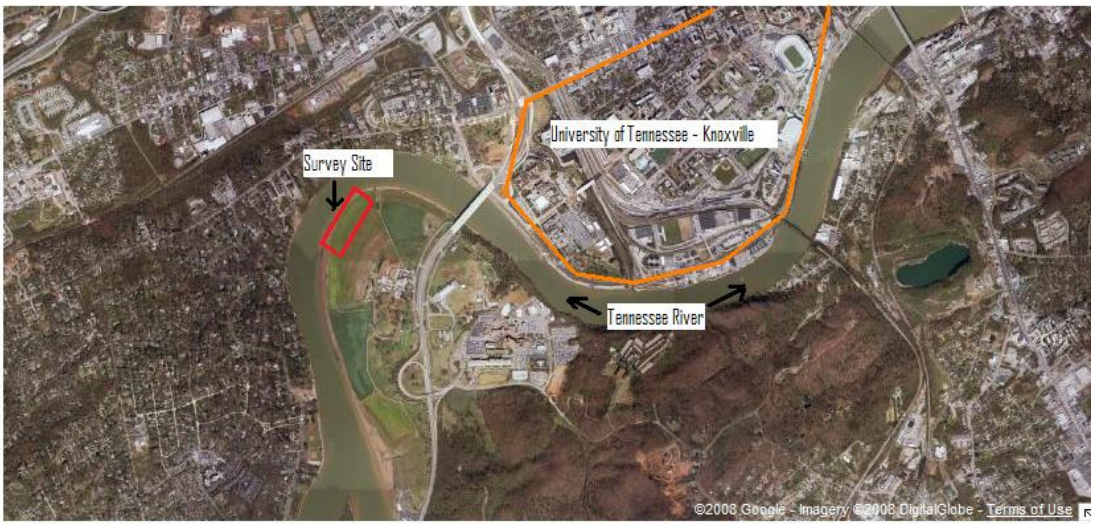

Figure 3.1. Site location. Survey site was on the flood plain of the Tennessee River, on the University of Tennessee Agriculture Campus.

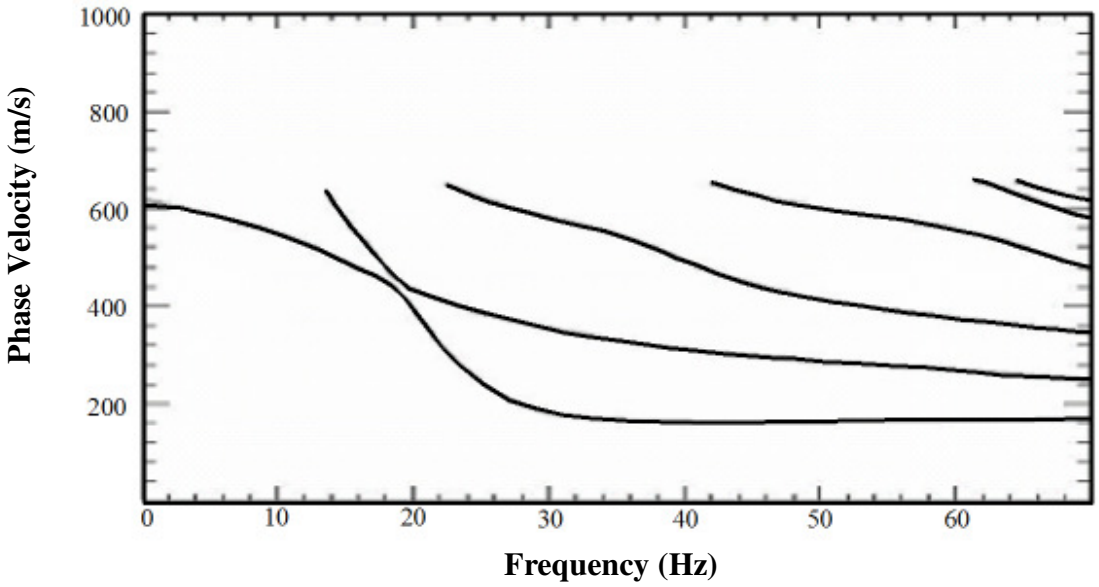

Figures 3.2. Example Rayleigh wave dispersion curves (no wave guide), fundamental mode and higher modes.

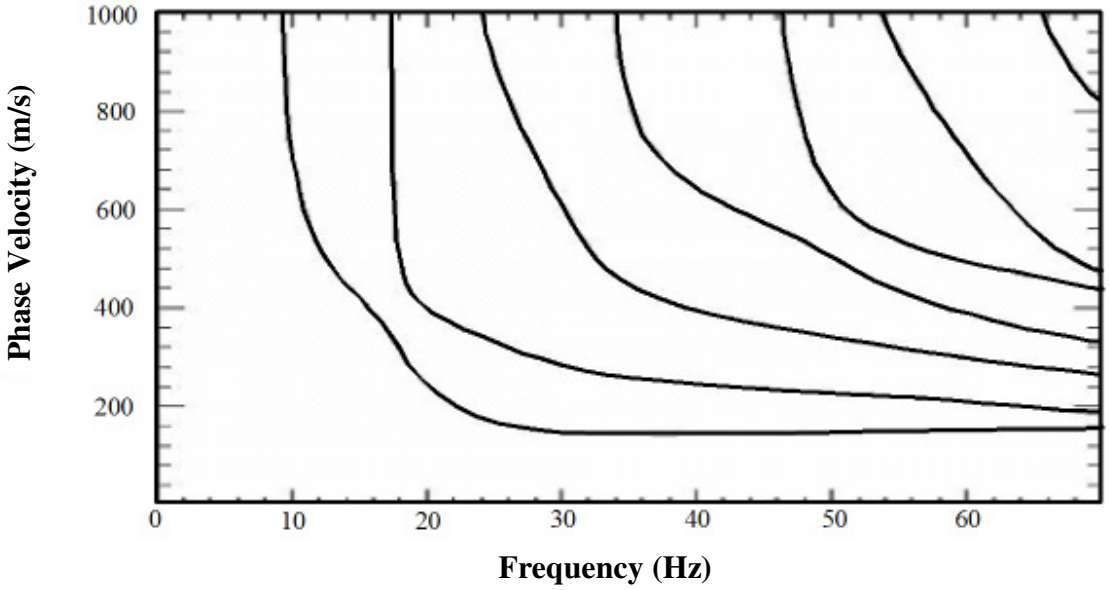

Figures 3.3. Example Rayleigh-Lamb wave dispersion curves (with wave guide), fundamental mode and higher modes. Subsurface velocities as in Fig. 3.2, but the effect of practically rigid bedrock is included. Notice cutoff in fundamental mode at ~10 Hz

Figure 3.4. Sources and receivers. Shallow holes were used to improve coupling.

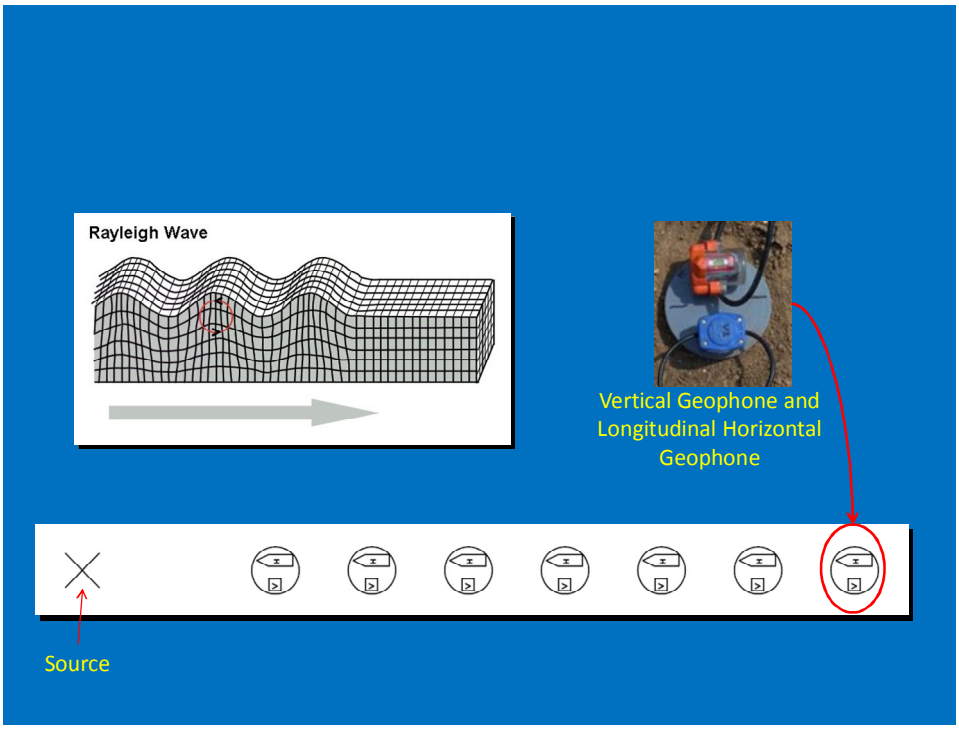

Figure 3.5. Measurement scheme of vertical and horizontal geophones for Rayleigh waves

Figure 3.6. Seismic sources. Top: sledge hammer and aluminum plate. Bottom left: 22.5 kg bag of sand. Bottom center: sledge hammer and 45° wooden block. Bottom right: ELECTRO-SEIS® vibrator.

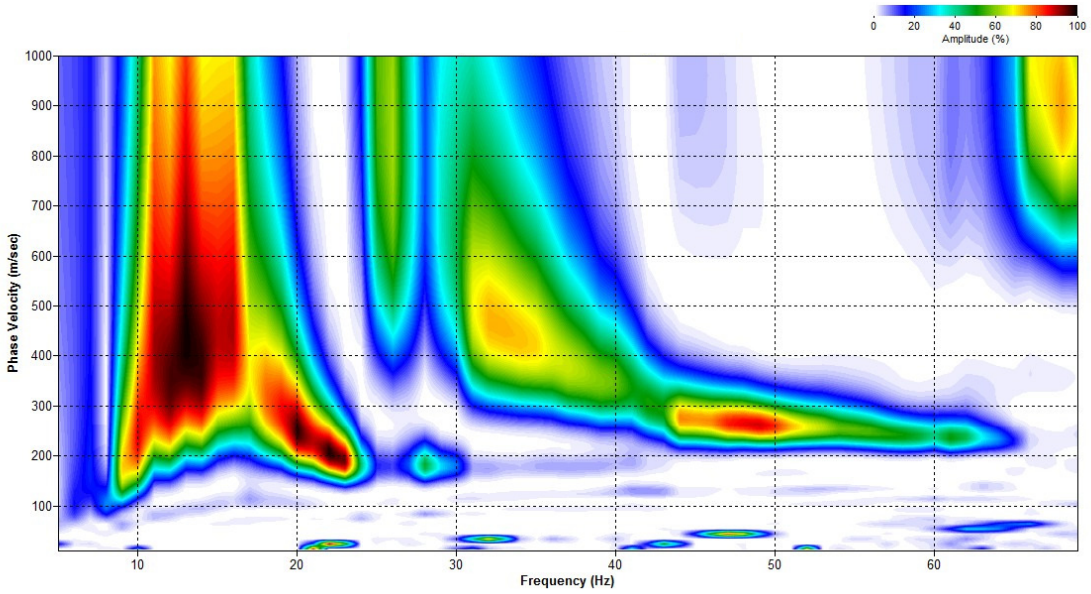

Figure 3.7. Dispersion image obtained using SurfSeis. Source offset of 5 m using sledge hammer and aluminum plate seismic source placed flat on the soil.

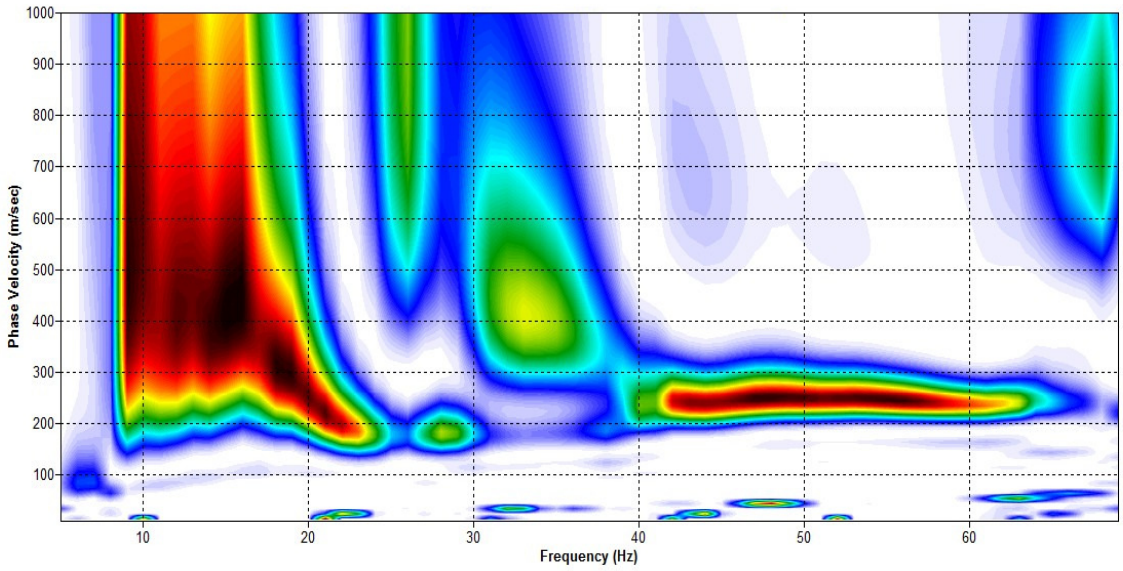

Figure 3.8. Dispersion image obtained using SurfSeis. Source offset of 5 m using 22.5 kg bag of sand seismic source dropped from a height of 1 m.

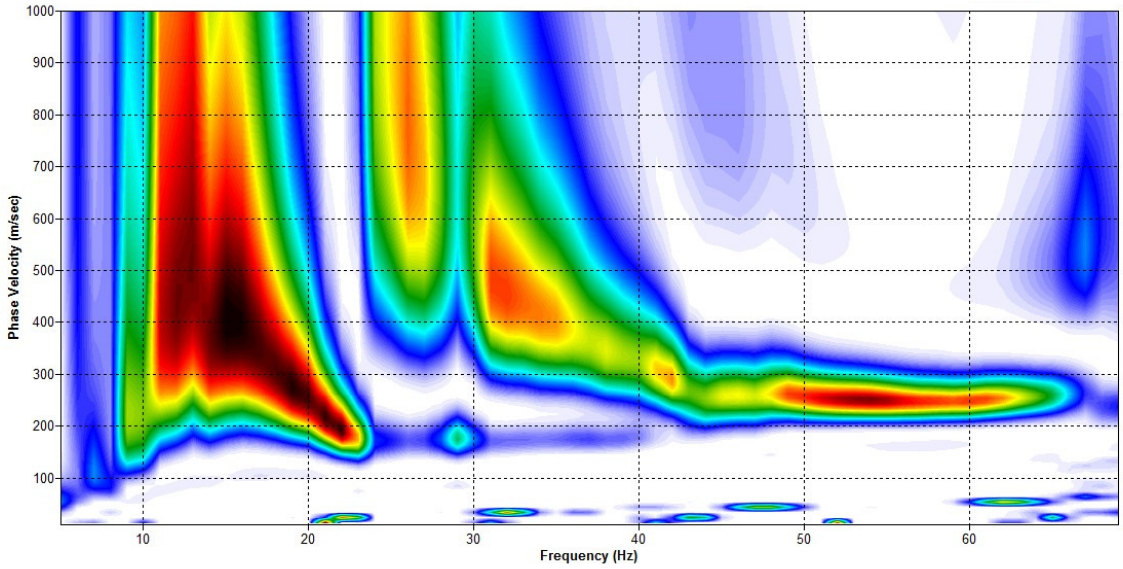

Figure 3.9. Dispersion image obtained using SurfSeis. Source offset of 5 m using sledge hammer and 45° wooden block seismic source.

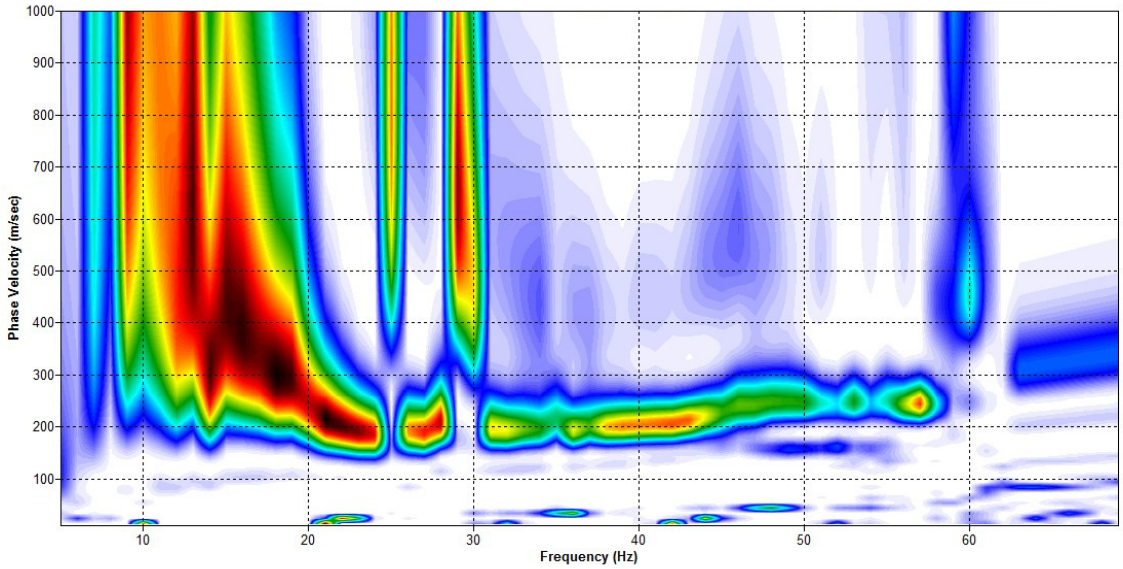

Figure 3.10. Dispersion image obtained using SurfSeis. Source offset of 5 m using ELECTRO-SEIS® vibrator seismic source.

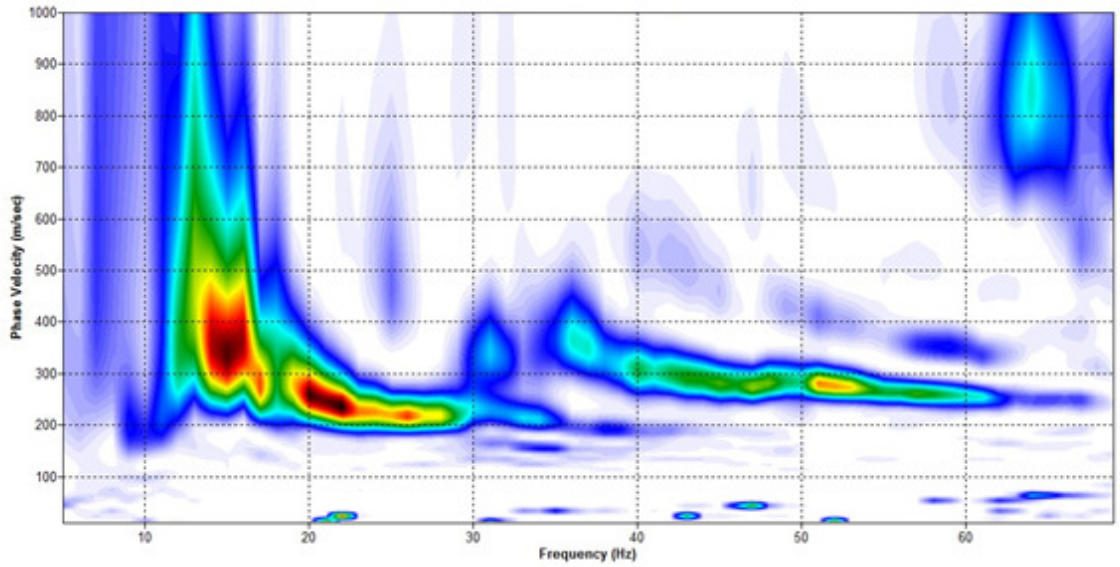

Figure 3.11. Dispersion image obtained using SurfSeis. Source offset of 1 m using hammer and 45° wooden block seismic source.

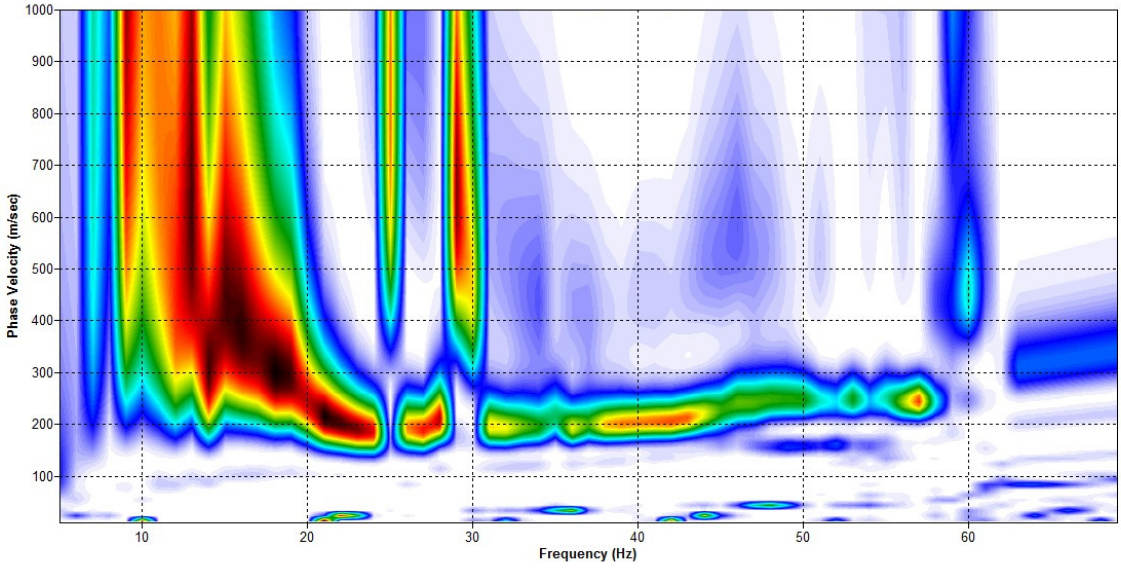

Figure 3.12. Dispersion image obtained using SurfSeis. Source offset of 16.5 m using 22.5 kg bag of sand seismic source.

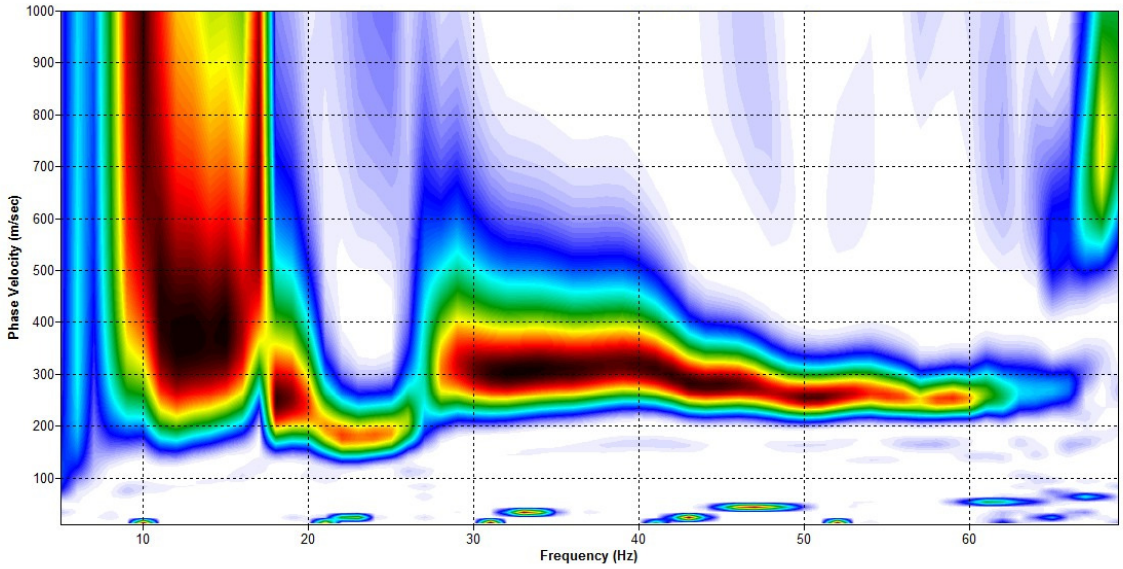

Figure 3.13. Dispersion image obtained using SurfSeis. Source offset of 28 m using 22.5 kg bag of sand seismic source.

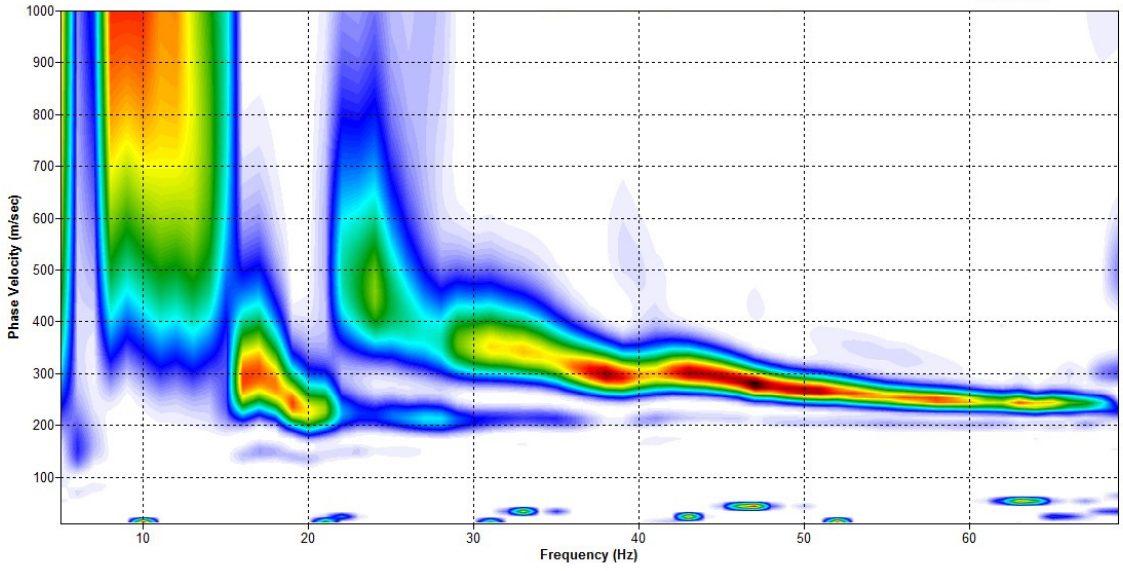

Figure 3.14. Horizontal, radially oriented geophone dispersion image obtained using SurfSeis. Source offset of 5 m using 22.5 kg bag of sand seismic source.

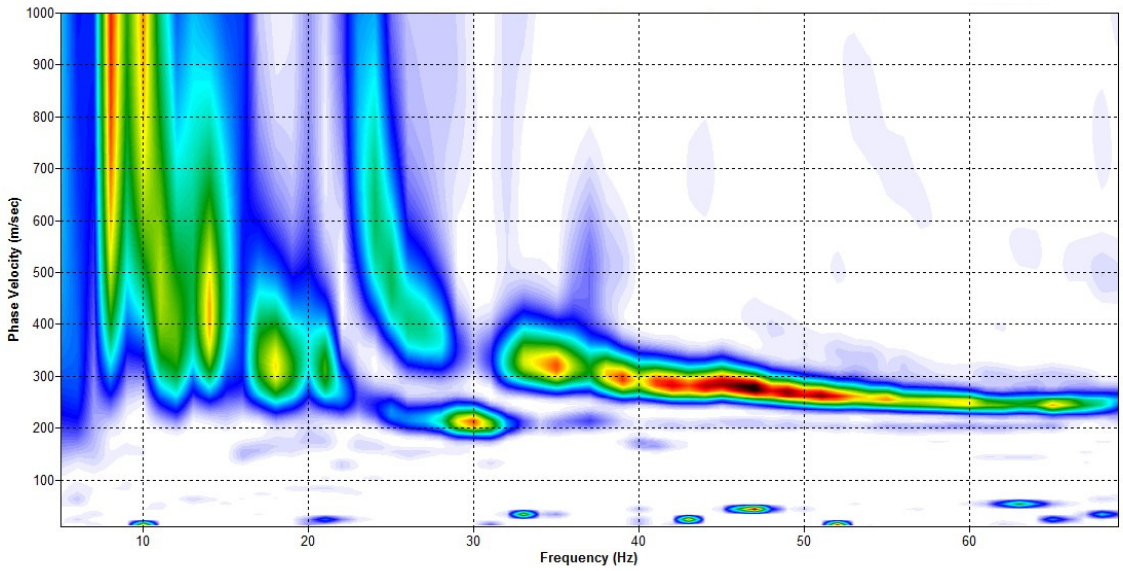

Figure 3.15. Horizontal, radially oriented geophone dispersion image obtained using SurfSeis. Source offset of 5 m using sledge hammer and 45° wooden block seismic source.

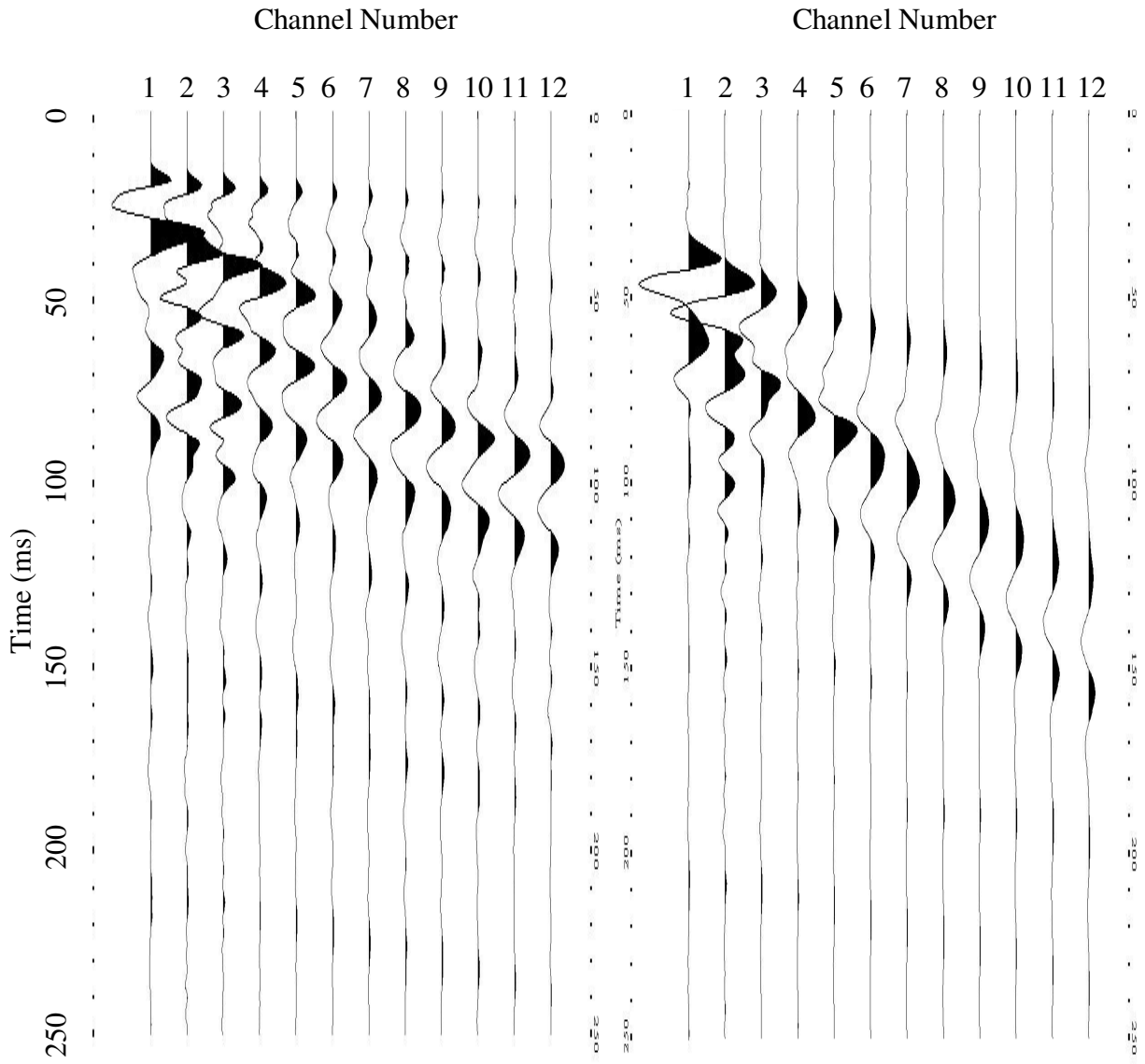

Figure 3.16. Seismic data example. One of 13 such records in the MASW data set. Left- vertical geophones. Right - Horizontal (radial) geophones. Shown are the first 250 ms from 1 second records.

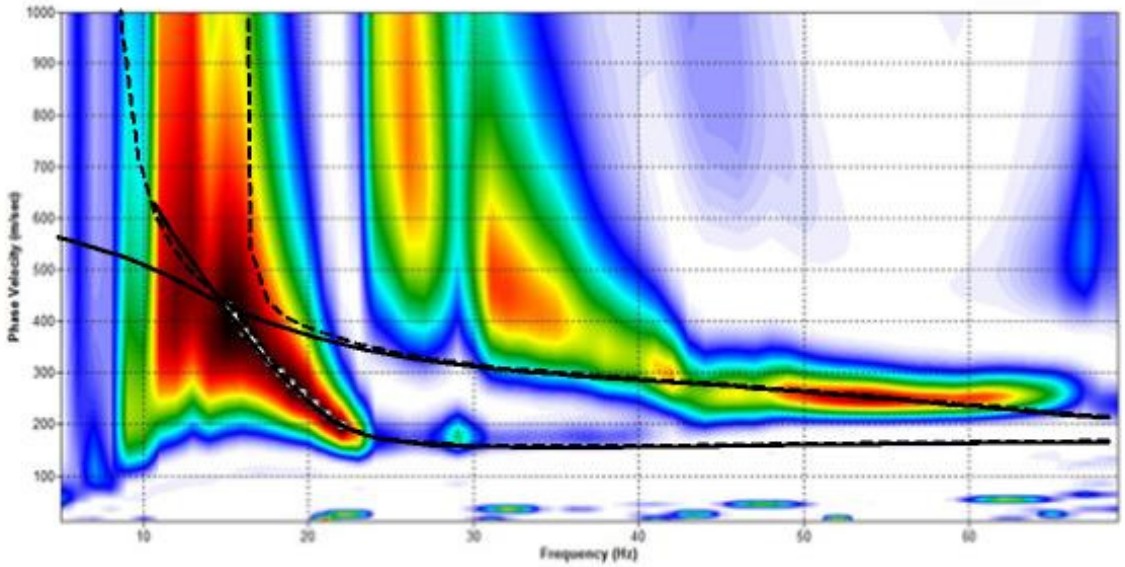

Figure 3.17. Fundamental mode dispersion curve (white squares) interepreted from the dispersion image for record #1. Solid lines- Rayleigh wave dispersion. Dashed lines- Rayleigh-Lamb dispersion. (see text)

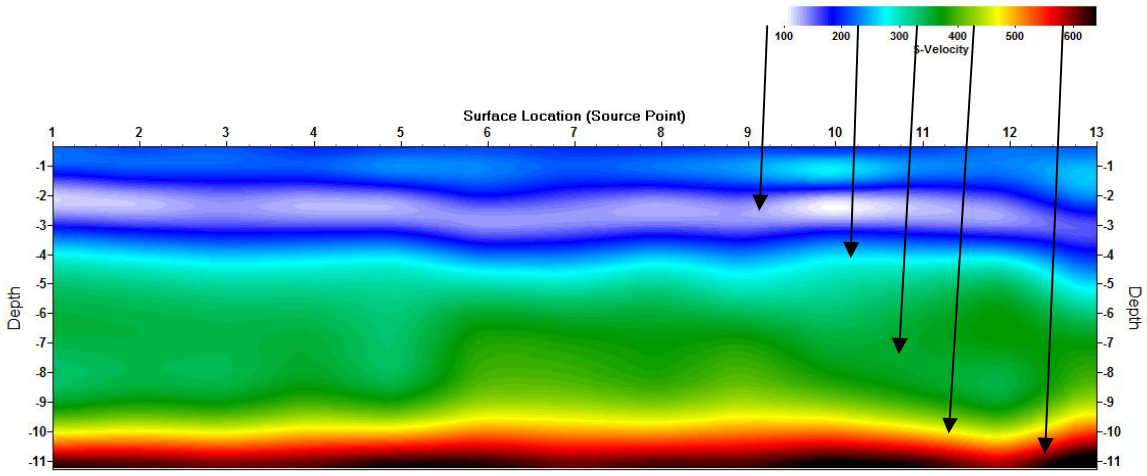

Figure 3.18. Result of MASW analysis: a 2-D shear velocity profile

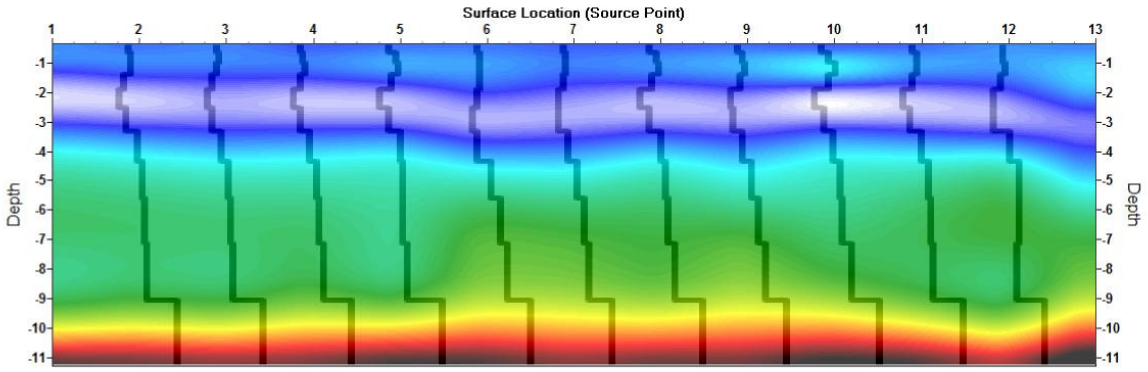

Figure 3.19. Shear velocity profile (Fig. 3.18) with overlay of individual 1-D inversion results.

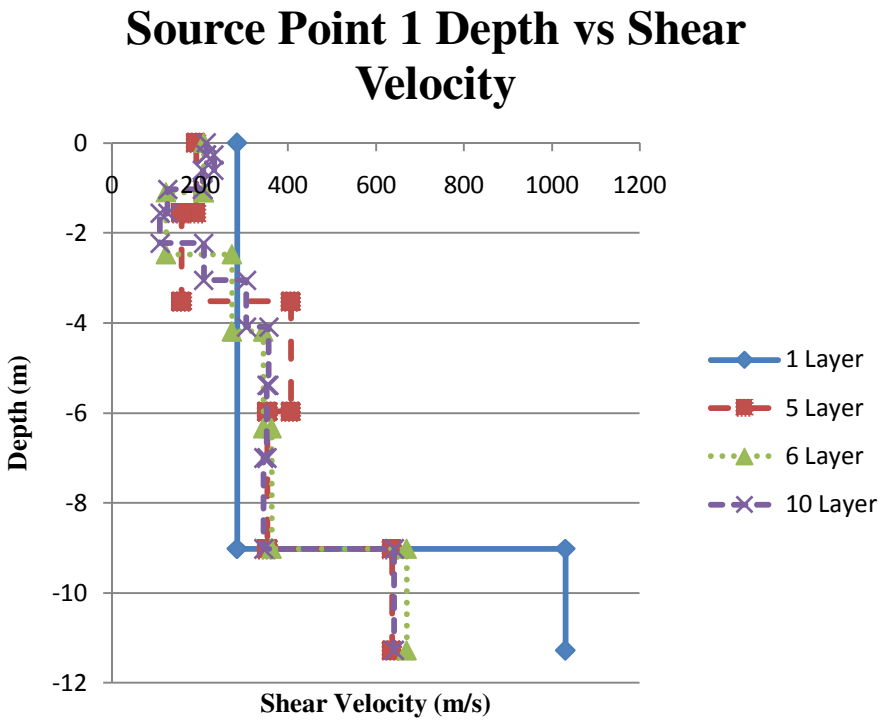

Figure 3.20. Shear velocity profile results based on number of layers at source point 1.

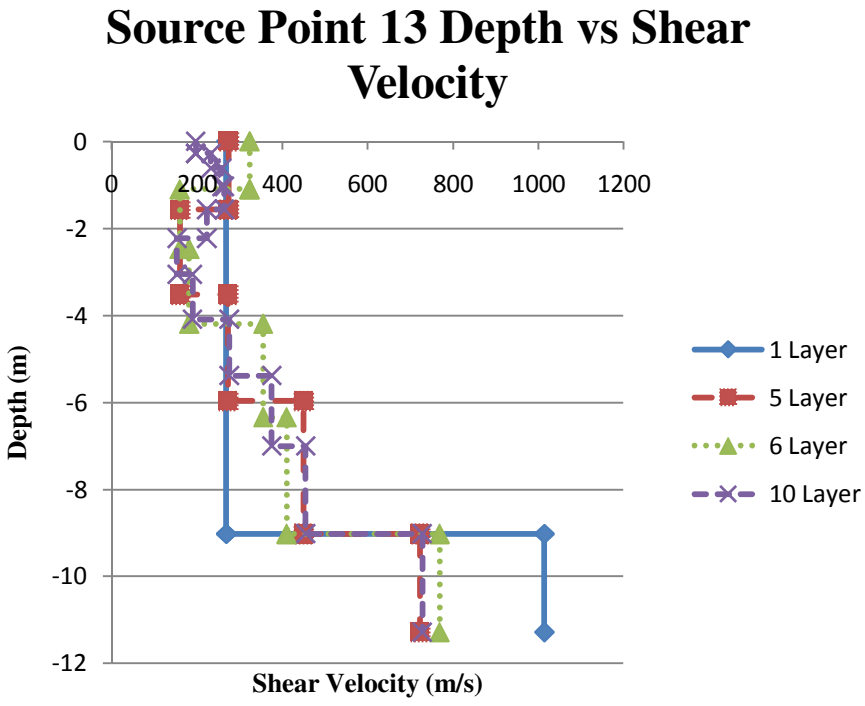

Figure 3.21. Shear velocity profile results based on number of layers at source point 13.

Chapter 4: Love Wave Dispersion, Analysis, and Modeling via the Multi-Channel Analysis of Surface Waves (MASW) Technique

My primary contributions to this paper include: (1) evaluation of the topic and development of the problem to study the optimum parameters for data collection at this specific site, (2) detailing the benefits of obtaining Love wave data in comparison to Rayleigh wave data, (3) obtaining and interpretation of published literature, (4) performing all field experiments and subsequent data analysis and interpretation, and (5) performing the writing necessary for manuscript preparation.

Abstract

The need to characterize sites where bedrock lies at shallow depth is common in geotechnical engineering. Here a site on the flood plain of the Tennessee River, where the soil is underlain by bedrock at relatively shallow depths, was characterized, using the MASW method. Usually, MASW utilizes fundamental mode Rayleigh wave dispersion to determine subsurface characteristics such as stratigraphy, shear velocity, and depth to bedrock. In this study, Love waves were used instead of Rayleigh waves, with improved results. A previous MASW study at the same site determined that the Rayleigh waves propagate in a waveguide, but was not effective at determining depth to bedrock. In contrast, the Love wave data leads to a precise interpretation of bedrock depth at 12.5 ± 0.5 m, taking into consideration the fundamental mode and 3 higher mode dispersion curves. The Love wave results suggest that shear wave velocity increases monotonically with depth, whereas the earlier Rayleigh wave study revealed a zone of relatively low velocity at a depth of approximately 1.5-3.0 m. Other published studies where Rayleigh and Love wave dispersion interpretations were compared have noted similar disparities between the Rayleigh and Love wave results, probably as a consequence of transverse anisotropy

in poorly consolidated sediments at shallow depths. Love wave dispersion images were easily interpreted in terms of fundamental mode dispersion, and significant, useful higher mode information was obtained as well. In contrast, Rayleigh wave dispersion images from the site were complicated and more difficult to interpret.

Introduction

Recent advances in surface wave data acquisition and inversion have provided valuable information regarding near-surface shear velocity profile characterization. Surface wave methods have evolved from dual channel analysis of surface waves (SASW) (Nazarian et al., 1983) to multi-channel-analysis of surface waves (MASW) (Park et al., 1999). Both of these near surface seismic wave techniques focused on determining shear wave velocity profiles of the subsurface using the fundamental mode Rayleigh wave dispersion. A number of case studies have been reported where Rayleigh wave dispersion and the MASW method were utilized in geophysical, geological, environmental, and geotechnical engineering projects. Ivanov et al. (2006) used MASW to delineate a shallow fault zone and dipping bedrock strata. Three-dimensional shear velocity mapping was accomplished using the MASW method at a military weapon test site in Arizona (Miller et al., 2003). MASW has been used to evaluate the effectiveness of a compaction operation conducted as a soil remediation monitoring tool at a construction site (Park et al., 2003)

Field investigations regarding the guidelines for Rayleigh wave data acquisition, such as receiver interval and array length, have been found to be applicable to Love wave data acquisition also (Eslick et al., 2008). The principal difference is that a horizontal seismic source

and horizontal geophones are needed to record Love waves. Love waves differ from Rayleigh waves (1) in that they depend only shear modulus and density, and not at all on Poisson's ratio, and (2) they do not propagate in a half-space (Adrianova, 1967). One or more low velocity layers are required (Love, 1911). Love wave dispersion is observed when a horizontal seismic source is actuated on a low velocity soil layer that overlies a half-space.

Safani et al. (2005) made several comparisons between Love and Rayleigh data at a location over shallow, fluvial deposits. They concluded that the Love wavefield appears to show a much higher signal-to-noise ratio than the Rayleigh wavefield over the same Earth. That is, it is less prone to scattering and (dominant) higher mode generation, and can be observed over a broader frequency range. Safani et al. (2005) also observed that in high-quality field data over unconsolidated soil, Rayleigh and Love wave models show different shear-wave velocities at similar depths, suggestive of transverse isotropy in shallow sediments. Rayleigh wave inversions for transversely anisotropic media produce shear wave velocities that are associated with the vertical direction, whereas Love waves are associated with shear wave velocities in the horizontal direction. Independence from Poisson's ratio is potentially an important advantage when analyzing Love wave data in stratified deposits. The goal of this study is to determine shear wave velocities for the flood plain of the Tennessee River via the MASW technique, but utilizing Love wave dispersion instead of Rayleigh wave dispersion.

Site Location

The site chosen for this study was located on the University of Tennessee, Knoxville agricultural farm as shown in Figure 4.1. The site lies in the flood plain on the Tennessee River,

where soft soils are expected to exhibit strong stratification over much stiffer bedrock. The bedrock is Knox dolomite (Cattermole, 1958). Christensen and Szymanski (1991) sampled the Knox dolomite in East Tennessee near the town of Thorn Hill, ~30 km from location of the present study, and made laboratory measurements of its seismic properties. They reported P-wave velocities at a range of confining pressures; however, they did not report S-wave velocity. At low confining pressure (10 MPa) they measured Vp = 6,120 m/s. Assuming that Poisson's ratio $\nu = 0.25$ for the dolomite, then Vs is estimated to be 3,530 m/s. Thus it is reasonable to expect that Vs for bedrock, on average, is ~3,500 m/s.

Studies of Rayleigh wave dispersion at the same location showed that Rayleigh waves do not propagate at frequencies lower than ~10 Hz (Figure 3.9). Also, the MASW dispersion images for Rayleigh waves are complicated and difficult to interpret. S-wave velocities in the soft soil layers are 5-10 times slower than the S-wave velocity in the Knox dolomite bedrock. In this situation, bedrock is effectively rigid, and the surface wave energy travels in a waveguide formed by the soil layers between bedrock and the free surface. Dispersion curves for waveguides having a free surface on one side and clamped on the other were published by Vorovich and Babeshko (1979). Example dispersion curves including fundamental and higher modes are presented in Figure 4.2 for Rayleigh waves and in Figure 4.3 for Love waves. In these figures, it can be seen that a cutoff frequency exists for both Rayleigh and Love wave propagation such that between DC and the cutoff frequency the surface waves do not propagate.

Survey Setup

The seismic data were acquired using a Geometrics model RX-48 seismograph to record both vertical and horizontal geophones. There were 48 geophones consisting of 24 verticals, which recorded Rayleigh waves, and additional 24 horizontals oriented transverse to the seismic profile to record Love waves. Pairs of vertical and horizontal geophones were mounted on circular steel plates (Figure 4.4). The seismic source was a sledge hammer striking a 45° wooden block at a source-offset distance of 5 meters from the nearest geophone. The 45° impact of the hammer onto the wooden block simultaneously excites both Rayleigh and Love waves. Here, the Rayleigh wave data were discussed in Chapter 3. Only the Love wave data collected from the horizontally oriented geophones was used for the present study.

Coupling between the geophones and the soil is an important factor in obtaining high-quality data. For this reason, the top 0.2 meter of topsoil was removed to ensure that no obvious organic material remained. Removing topsoil and organic material eliminates the damping effects of the sod and possible voids between the geophone plates and the soil. Both the geophones and seismic source were placed in shallow scrapes spaced at 1-meter intervals, beginning with the 5 meter source offset. Figure 4.5 illustrates the source and geophone locations, and hammer and 45° angle wooden block seismic source. An example of the seismic data collected using this field setup is presented in Figure 4.6

Love Wave MASW Survey

The MASW technique usually involves moving the source and geophones together in a roll along pattern (Dobrin and Savit, 1988), which in this case advances everything in 1 meter

increments from one source point to the next. For the MASW analysis, subsets of 12 geophones were extracted from the 24 geophone array, yielding 13 seismograms with seismic traces with 12 geophones in each. The 13 seismograms span a MASW profile length of 13 m.

The MASW seismic data were analyzed using SurfSeis software (Kansas Geological Survey (1998, 2006) to produce dispersion images. To begin, data from the entire 24 geophone array was analyzed as one seismogram to obtain baseline dispersion information. The baseline dispersion image is shown in Figure 4.7, where white squares show the interpreted phase velocities at selected frequencies. The baseline dispersion data (white squares) was inverted using the program SURF96 from the Computer Programs in Seismology (CPS) software package (Hermann, 1996). SurfSeis was not used for Love wave data, because it is capable of inverting only fundamental mode Rayleigh wave data. In contrast, CPS includes programs for inverting both Rayleigh and Love wave dispersion data, taking into account multiple modes simultaneously. The results of inverting the baseline dispersion data are presented in Figure 4.8, where it can be seen that both the fundamental mode and first higher mode, which is weakly visible in the dispersion image, are satisfied. Subsequently, the 13 seismograms were analyzed to study the variability of Love wave dispersion and shear wave velocity along the 13 m profile. The results are presented in Table 1 and Figure 4.9. Here, 32 layers were used in the inversion, because slight differences were noted in the higher modes when the inversions were done using 10 layers. The inversions were based only on fundamental mode data, but the results satisfied the observed dispersion at least to the third higher mode (Figure 4.10).

As noted by Safani et al. (2005), a Love wave experiment is less prone to dominant higher mode generation than a Rayleigh wave experiment (compare Figure 4.8 to Figure 3.9).

The higher modes, weak or invisible in the dispersion images, were enhanced by summing the 13 dispersion images to produce the stacked dispersion image shown in Figure 4.10. The second and third higher modes can be seen in the stacked image. The higher mode data were not included in the inversion, but inversion of the fundamental mode dispersion data satisfies all of the visible higher modes.

Constraints on Depth to Bedrock

The model used for CPS inversion of the Love wave dispersion data is based on a model consisting of homogeneous, isotropic soil layers over bedrock. The bedrock is much stiffer than the soil layers but not completely rigid. The properties of bedrock were appropriate for the Knox dolomite (Vp = 6,120 m/s, Vs = 3,500 m/s), but the depth to bedrock was not known. Instead, depth to bedrock was included in the inversion process. Considering only the fundamental mode Love wave dispersion data, the depth to bedrock is very poorly constrained. Changing the depth to bedrock causes the velocities in the soil layers to change, but the resulting fundamental mode dispersion curve remains the same. Important, additional constraints on bedrock depth come from observations of the higher modes. Changing the depth to bedrock changes the spacing between the fundamental and higher mode dispersion curves in Figures 4.8 and 4.10. Thus, if the depth to bedrock is wrong in the model, the fundamental mode dispersion is satisfied by the model, but the higher modes are not. A range of bedrock depths is included in the dispersion curves of Figures 4.8 and 4.10. Here, the spacing of the higher mode dispersion curves constrains bedrock to a narrow range of depths from 12 to 13 m.

Conclusions

1. Love wave dispersion images are more easily interpreted than Rayleigh dispersion images, largely because Love waves are less prone to dominant higher mode generation than Rayleigh waves.
2. Inversion of the Rayleigh and Love wave dispersion data leads to somewhat different shear velocity profiles in the poorly consolidated soil. The effect probably relates to transverse anisotropy in the strata.
3. Joint MASW analysis of Rayleigh and Love wave dispersion data is problematic due to the likelihood of significant transverse anisotropy in poorly consolidated sediments. A new inversion algorithm is needed, which explicitly includes the effects of transverse anisotropy.
4. In a shallow bedrock situation, Love wave dispersion data have good capability for determining the depth to bedrock, through observations of the higher modes, in addition to the fundamental mode. The fundamental mode alone provides little constraint on this important parameter.

References

Adrianova, Z.S., Keilis-Borok, V.I., Levshin, A.L., and Neigauz, M.G., 1967, "Seismic Love Waves," Consultants Bureau, New York, 91 pp.

Barton, N.R., 2008, "Rock quality, seismic velocity, attenuation and anisotropy," T & F Books, London, 729 pp.

Cattermole, J.M., 1958, Geology of the Knoxville Quadrangle, Tennessee, Geologic Quadrangle Map GQ-115, U.S. Geologic Survey

Christensen, N.I. and Szymanski, D.L., 1991, "Seismic properties and the origin of reflectivity from a classic Paleozoic sedimentary sequence, Valley and Ridge province, southern Appalachians," GSA Bull. 103, 277-289.

Dobrin, M.B, and Savit, C.H., 1988, Introduction to Geophysical Prospecting, McGraw-Hill, New York, 867 pp.

Dobroka, M., Gyulai, A., Ormos. T., Csokas, J., and Dresen, L., 1991, Joint inversion of seismic and geoelectric data in an underground coal mine, Geophys. Prosp. 39, 643-665

Eslick, R., Tsoflias, G., and Steeples, D., 2008, "Field investigation of Love waves in near-surface seismology," Geophysics, 73(3), G1-G5

Hering, A., Misiek, R., Gyulai, A., Ormos., T., Dobroka, M., and Dresen, L., 1995, A joint inversion algorithm to process geoelectric and surface wave data, Part I: Basic Ideas, Geophys. Prosp., 43, 135-156

Hermann, R. B., 1996, Computer Programs in Seismology ver. 3.30, distributed by Saint Louis University, http://www.eas.slu.edu/People/RBHerrmann/ComputerPrograms.html

Ivanov, J., Miller, R.D., Lacombe, P., Johnson, C.D., and Lane Jr., J.W., 2006, Delineating a shallow fault zone and dipping bedrock strata using multi-channel analysis of surface waves with a land streamer, Geophysics, 71(5), A39-A42

Kansas Geological Survey (KGS), 2006, SurfSeis [computer software], Ver. 2.05

Kansas Geological Survey (KGS), 1998, Introduction to MASW acquisition and processing, http://www.kgs.ku.edu/software/surfseis/masw.html

Love, A.E.H., 1911. Some Problems of Geodynamics. Cambridge University Press.

Lambe, T.W., and Whitman, R.V., 1969, Soil Mechanics, John Wiley & Sons, New York, 553 pp.

Miller, R.D., Anderson, T.S., Ivanov, J., Davis, J.C., Olea, R., Park, C.B., Steeples, D.W., Moran, M.L., and Xia J., 2003, 3-D characterization of seismic properties at the Smart Weapons Test Range, YPG [Exp. Abs.]: Soc. Expl. Geophys., NSG 2.3

Misiek, R., Liebig, A., Gyulai, A., Ormos, T., Dobroka, M., and Dresen, L., 1997, A joint inversion algorithm to process geoelectric and surface wave seismic data, Part II: Applications, Geophys. Prosp., 45, 65-85

Nazarian, S., Stokoe, K.H., II, and Hudson, W. R., 1983, Use of spectral analysis of surface waves method for determination of moduli and thicknesses of pavement systems: Transport. Res. Record, 930, 38-45

Park, C.B., and R.D. Miller, 2003, MASW for shear wave velocity evaluation of soil before and after deep dynamic compaction operations: Kansas Geological Survey Open-file Report 2003-64.

Park, C.B., Miller, R.D., and Xia, J., 1999, Multi-channel analysis of surface waves, Geophysics, 64(3), 800-808

Safani, J., O'Neill, A., Matsuoka, T., and Sanada, Y., 2005, Applications of Love Wave Dispersion for Improved Shear-wave Velocity Imaging, Journal of Environmental & Engineering Geophysics, Vol. 10, Iss. 2., 135-150

Stein, S., and Wysession, M., 2003, An introduction to seismology, earthquakes, and earth structure: Blackwell Scientific Publications, Inc.

Vorovich, V.V, and Babeshko, V.A., 1979, Mixed dynamic problems of elasticity for non-classical domains, Moscow, Nauka, 320 pp. (in Russian)

Appendix

Tables

Table 4.1. Shear velocities (m/s) as a function of source point and depth for a 33 layer inversion. Knox dolomite bedrock is at the base of the soft sediment layers. The depth column shows depth to the bottom of the layer.

	Source Point												
Depth (m)	**1**	**2**	**3**	**4**	**5**	**6**	**7**	**8**	**9**	**10**	**11**	**12**	**13**
-0.39	107	108	108	113	112	113	114	113	112	114	114	113	119
-0.78	138	138	138	141	142	143	143	142	143	142	143	141	144
-1.17	171	174	175	173	177	178	178	177	178	174	175	175	171
-1.56	209	210	210	210	211	212	212	213	213	210	212	210	202
-1.95	242	240	239	239	240	241	240	241	241	239	241	239	225
-2.34	265	261	260	259	261	261	261	262	262	258	259	258	241
-2.73	274	274	273	271	271	272	271	274	272	271	272	271	251
-3.13	282	281	280	279	279	281	279	282	280	280	281	279	258
-3.52	289	286	284	285	283	284	282	287	283	286	286	284	263
-3.91	284	284	284	282	282	283	282	284	282	284	283	282	263
-4.30	284	286	284	284	283	284	282	285	283	284	285	284	266
-4.69	281	283	283	283	281	282	281	285	281	284	284	283	267
-5.08	279	282	282	282	281	282	280	284	280	284	283	283	271
-5.47	276	280	280	280	279	280	279	282	279	282	281	281	273
-5.86	278	282	282	281	282	282	281	282	281	283	283	282	278
-6.25	279	284	283	283	283	283	283	282	283	283	284	284	283
-7.03	288	288	287	288	289	288	289	287	288	290	289	290	296
-7.42	298	299	298	297	299	297	298	295	298	297	297	298	307
-7.81	303	304	303	302	305	302	304	300	304	303	302	303	316
-8.20	309	312	313	310	314	311	313	307	314	310	310	312	326
-8.59	326	324	324	322	325	322	324	320	325	323	322	324	339
-8.98	338	334	334	333	337	333	336	330	337	333	333	334	351
-9.38	347	345	345	342	347	343	346	339	347	342	342	343	362
-9.77	358	358	357	354	359	354	358	350	359	353	353	355	374
-10.16	371	369	368	365	371	366	370	361	370	365	365	367	385
-10.55	385	382	381	379	384	380	383	374	383	378	378	380	397
-10.94	397	394	394	391	396	392	395	387	395	390	390	392	408
-11.33	410	408	408	405	410	405	408	402	409	404	404	406	420
-11.72	422	421	420	418	422	418	421	416	422	418	418	419	431
-12.11	438	433	433	433	435	433	435	432	435	433	433	434	443
-12.50	452	448	448	448	449	448	448	447	448	448	448	448	454
	3524	3524	3524	3524	3524	3524	3524	3524	3524	3524	3524	3524	3524

Figures

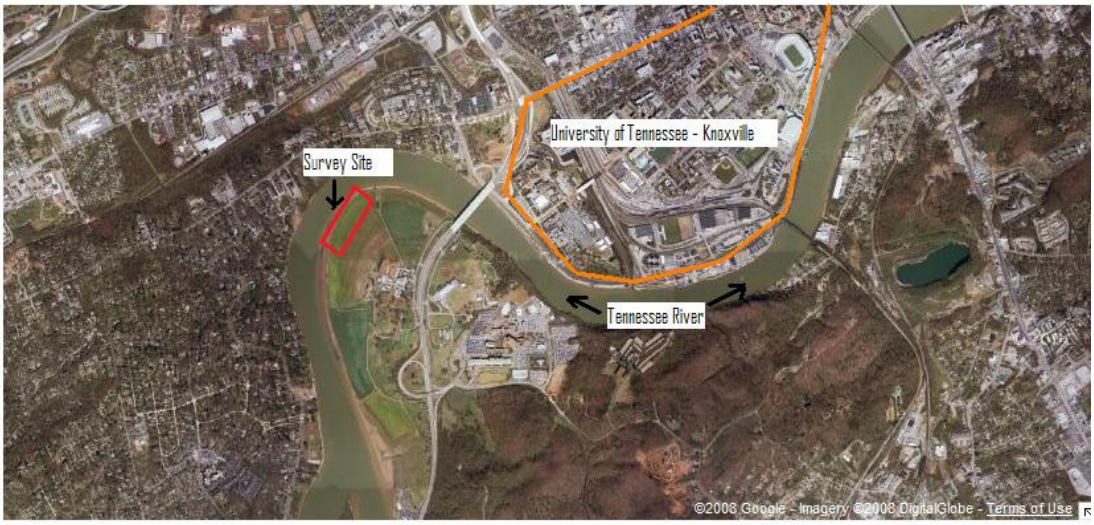

Figure 4.1. Surface wave data were recorded on the flood plain of the Tennessee River at Knoxville, TN.

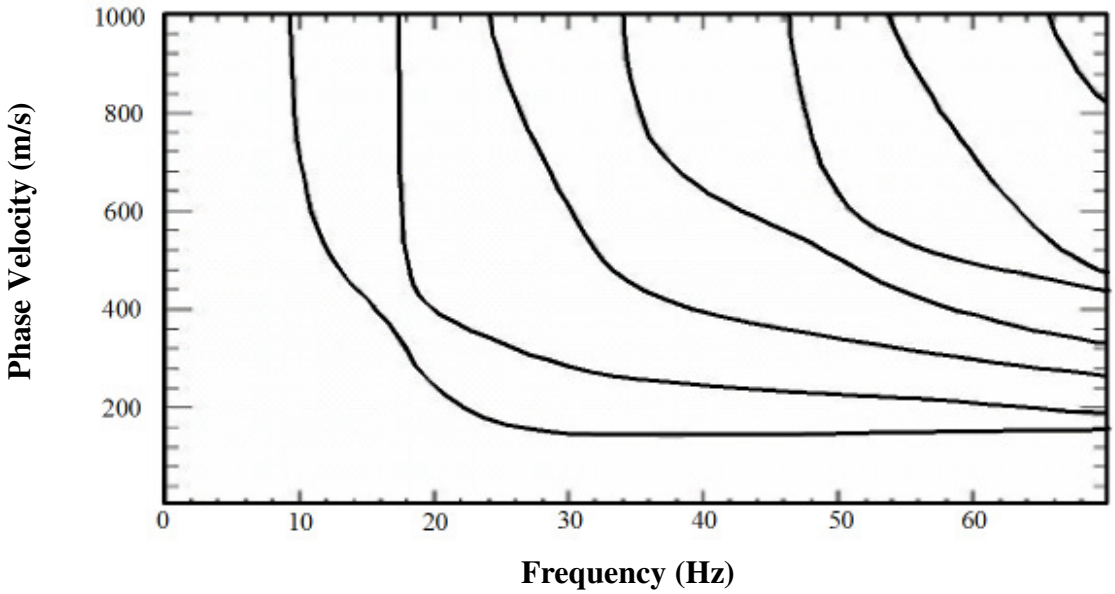

Figure 4.2. Example Rayleigh-Lamb (waveguide) wave dispersion curves, fundamental mode and higher modes. Results in Table 3.1 (i.e. number of soil layers, shear velocities, depth to bedrock) used for starting model except Knox Dolomite properties were used for the bottom layer.

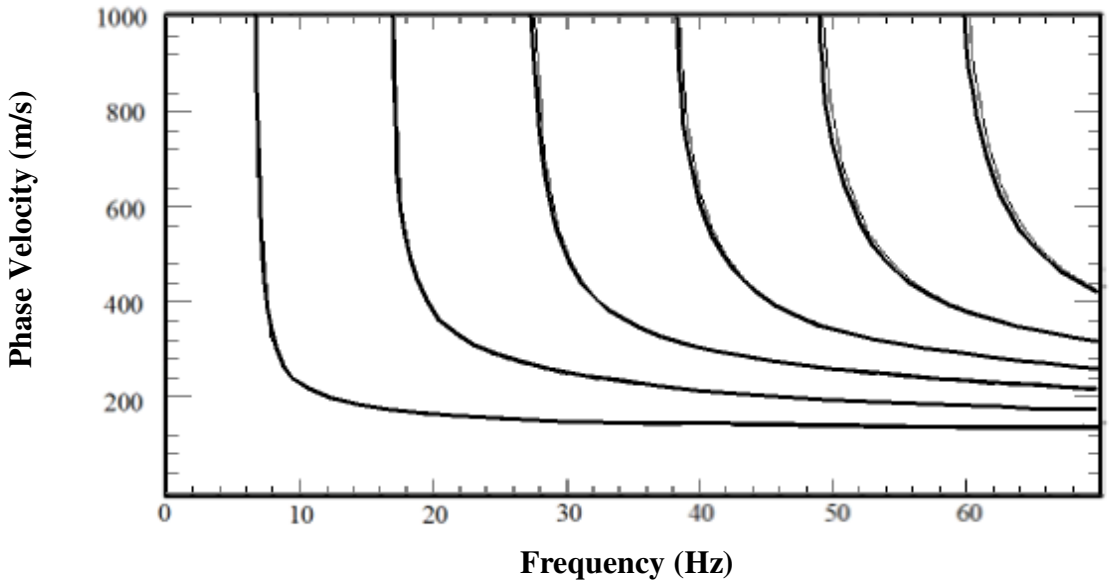

Figure 4.3. Example Love wave dispersion curves, fundamental mode and five higher modes. Starting model used 10 m depth to bedrock, 125 m/s near surface shear velocity monotonically increasing to 450 m/s for deep shear velocity.

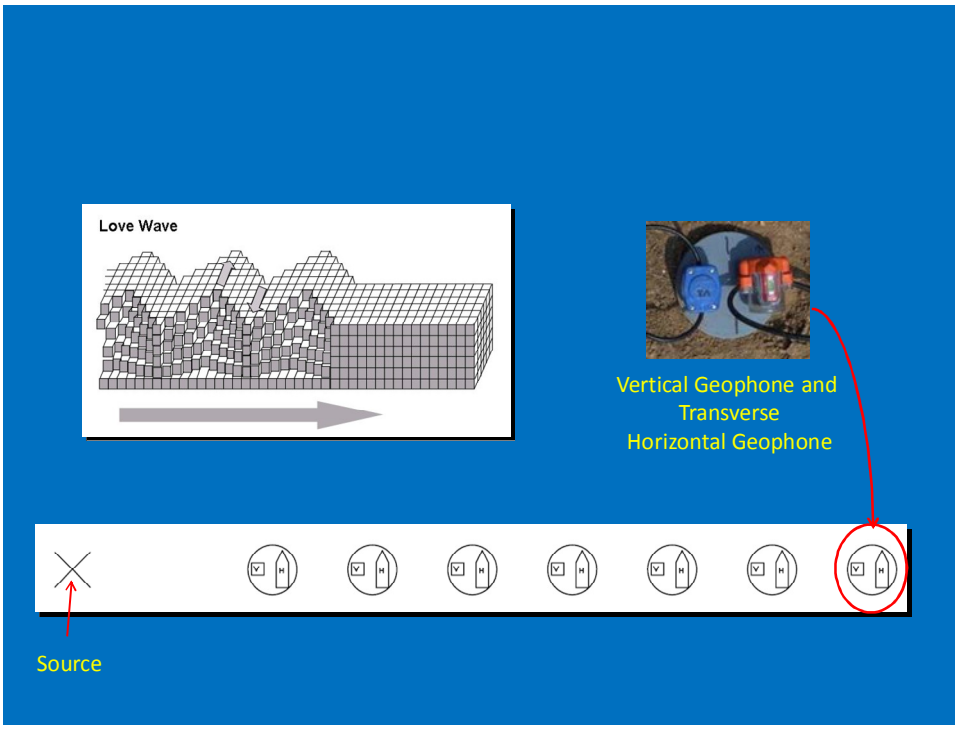

Figure 4.4. Measurement scheme for vertical and horizontal geophones for Love wave detection

Figure 4.5. Left: Hammer and 45° wooden block source, Right: Geophone coupling location

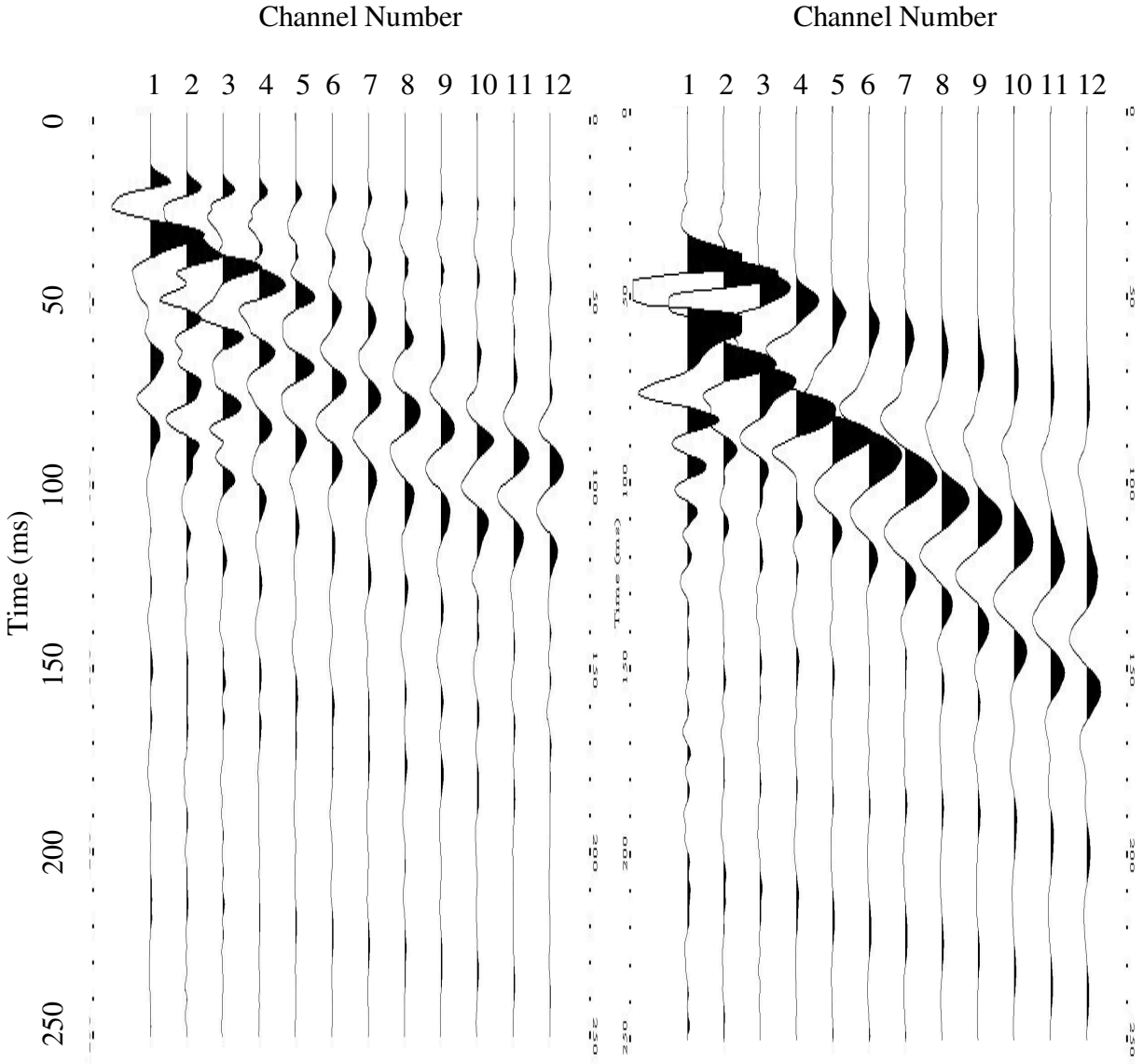

Figure 4.6. Seismic data example. Left - vertical geophones. Right - Horizontal (transverse) geophones. Shown are the first 250 ms from 1 second records.

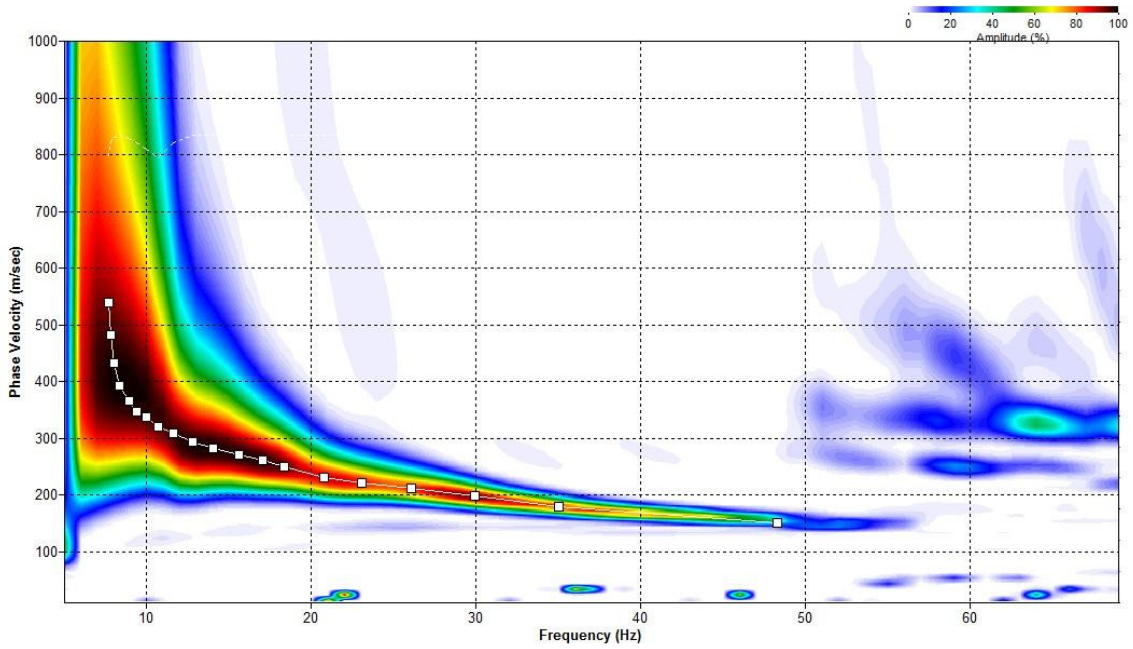

Figure 4.7. Baseline dispersion image obtained by analyzing the data from 24 horizontal geophones as a single seismic data record. White squares show the phase velocities interpreted at selected frequencies for the fundamental mode. Compare to the corresponding dispersion image for Rayleigh wave data (Fig. 3.9).

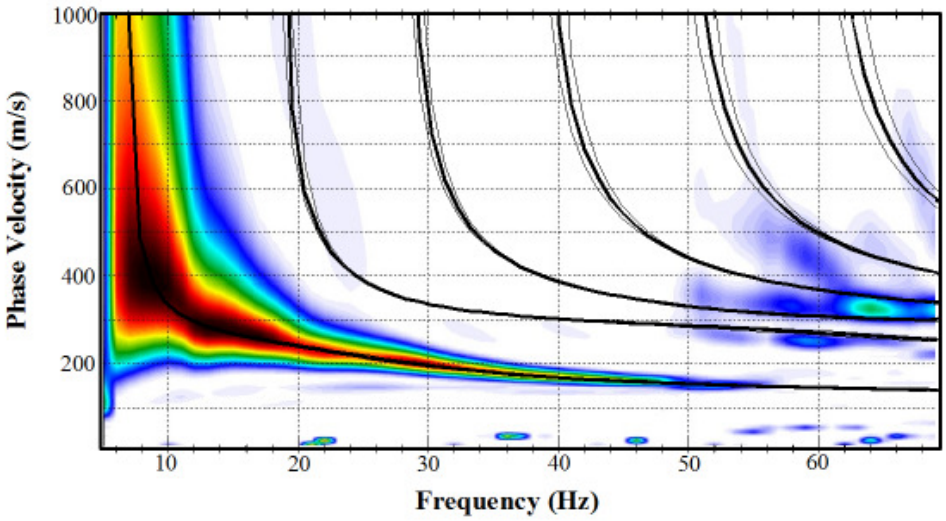

Figure 4.8. Baseline dispersion image (Fig. 4.8) with fundamental and higher mode Love wave dispersion curves (heavy black lines) that result from inversion of the dispersion data (white squares in Fig. 4.8). Note that the first higher mode, weakly visible in the dispersion image, is also satisfied by inversion of only the fundamental mode data. Thin black lines right and left of the heavy black dispersion curves are for bedrock depths at 12 and 13 m, respectively. Heavy curves are for 12.5 m bedrock depth.

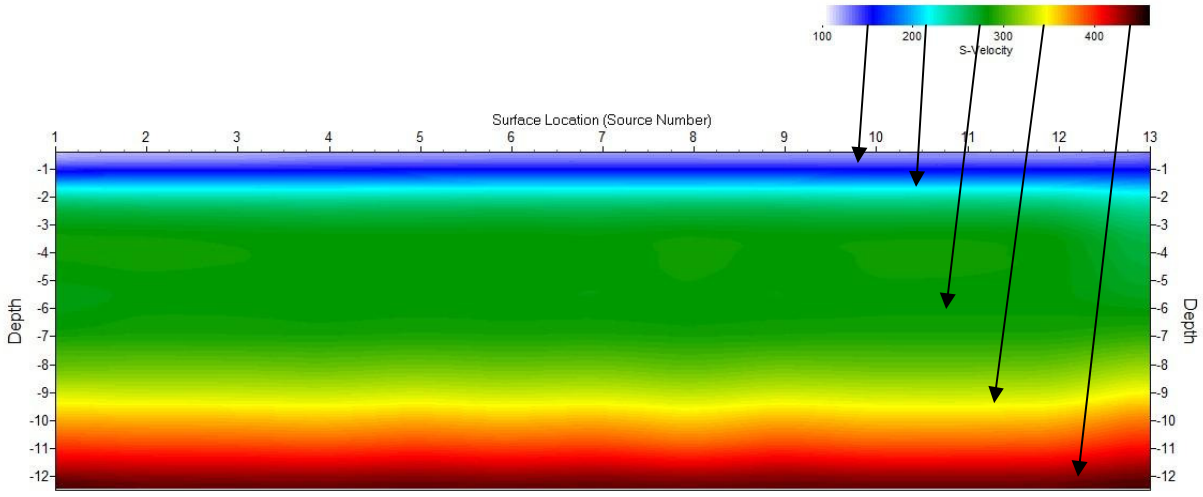

Figure 4.9. Result of MASW analysis. The profile has a horizontal exaggeration of approximately 4X. The distance from the left edge to the right edge is 12 m, almost the same as the vertical span of 12.5 m.

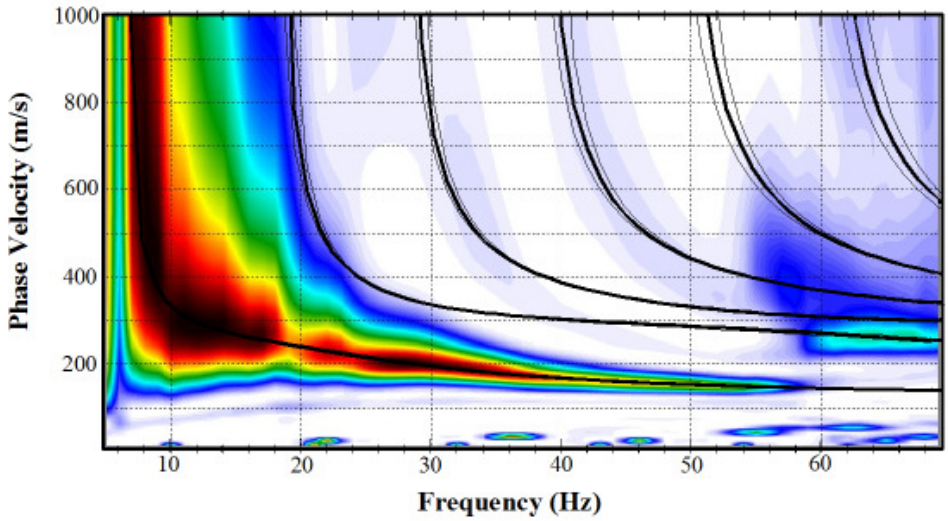

Figure 4.10. Stack of 13 individual dispersion images to enhance the higher modes. The first higher mode, visible in Figure 4.9 is no can no longer be seen, but dispersion of the second and third higher modes is revealed. Note that inversion of only the fundamental mode data also satisfies the visible higher modes.

Conclusions and Recommendations for Future Research

Conclusions

1. Bedrock was not detected by inversion of the fundamental mode Rayleigh wave dispersion data in SurfSeis.

2. Inversion of the dispersion curves in this type of situation may be improved by using a different model, with the soil layers forming a wave guide that is clamped on the bottom by semi-rigid bedrock (Rayleigh-Lamb waves) instead of classical Rayleigh waves.
3. The ELECTRO-SEIS® vibrator produced the best dispersion image for the fundamental mode. The vibrator, however, was less effective at exciting higher mode Rayleigh waves and was cumbersome to use in the field. The best source overall was the simple sledge hammer and wooden block.
4. Concerning the optimum source offset distance, the equation proposed by Zhang et al. (2004) is useful in the case of soil over shallow bedrock (Rayleigh-Lamb waves), but the depth to bedrock is the principal variable controlling the optimum offset.
5. Bedrock was not detected by inversion of the fundamental mode Rayleigh wave dispersion data in SurfSeis.

6. Inversion of the dispersion curves in this type of situation may be improved by using a different model, with the soil layers forming a wave guide that is clamped on the bottom by semi-rigid bedrock (Rayleigh-Lamb waves) instead of classical Rayleigh waves.
7. The ELECTRO-SEIS® vibrator produced the best dispersion image for the fundamental mode. The vibrator, however, was less effective at exciting higher mode Rayleigh waves

and was cumbersome to use in the field. The best source overall was the simple sledge hammer and wooden block.

8. Concerning the optimum source offset distance, the equation proposed by Zhang et al. (2004) is useful in the case of soil over shallow bedrock (Rayleigh-Lamb waves), but the depth to bedrock is the principal variable controlling the optimum offset.

9. Rayleigh wave dispersion can be measured using either vertical or horizontal (radial) geophones. The vertical data are somewhat better than the horizontal, and there is little to be gained by using both.

10. Fundamental mode Rayleigh wave dispersion data can be explained using a relatively small number of soil layers. The resolution of the MASW technique is not improved by increasing the number of layers in the soil used the inversion process.

11. Love wave dispersion images are more easily interpreted than Rayleigh dispersion images, largely because Love waves are less prone to dominant higher mode generation than Rayleigh waves.

12. Inversion of the Rayleigh and Love wave dispersion data leads to somewhat different shear velocity profiles in the poorly consolidated soil. The effect probably relates to transverse anisotropy in the strata.

13. Joint MASW analysis of Rayleigh and Love wave dispersion data is problematic due to the likelihood of significant transverse anisotropy in poorly consolidated sediments. A new inversion algorithm is needed, which explicitly includes the effects of transverse anisotropy.

14. In a shallow bedrock situation, Love wave dispersion data have good capability for determining the depth to bedrock, through observations of the higher modes, in addition to the fundamental mode. The fundamental mode alone provides little constraint on this important parameter.

Recommendations for Future Research

1. Simultaneous inversion of both Rayleigh and Love wave dispersion curves.

2. Study the effects of Poisson's ratio (i.e. P-wave velocity) on the inversion process in the case of Rayleigh-Lamb waves.

Vita

James David Lane, Jr. was born in Virginia Beach, VA on April 9, 1979. He was raised in Stafford County, VA and attended grade school at Ferry Farm Elementary and junior high school at Gayle Middle School. He graduated from Stafford Senior High School in 1997. He attended Germanna Community College in Fredericksburg, VA with a major in Business Administration. From there, he attended the University of Tennessee, Knoxville and received a B.S. in Civil Engineering in the fall of 2006 and intends on graduating with an M.S. in Civil Engineering with an emphasis in Geotechnical Engineering in the fall of 2009. Dave is currently employed as an Environmental Engineer with the Tennessee Valley Authority in the Environmental Engineering Services East organization.